In Situ UV-Visible Plasmon Resonance Spectroscopic Assessment of Oxygen and Hydrogen Adsorption Location on Supported Gold Catalysts

Priya D. Srinivasan,[a,b] Hongda Zhu, [a] and Juan J. Bravo-Suárez [a,b,*]

[a] *Center for Environmentally Beneficial Catalysis, The University of Kansas, Lawrence, KS, 66047, USA*

[b] *Department of Chemical & Petroleum Engineering, The University of Kansas, Lawrence, KS, 66045, USA*

* Corresponding author at: Center for Environmentally Beneficial Catalysis, The University of Kansas, Lawrence, KS 66047, USA.

E-mail address: jjbravo@ku.edu (J. J. Bravo-Suárez)

Abstract

Here we report an in situ UV-Visible spectroscopy study of O_2 and H_2 adsorption on small gold nanoparticles supported on SiO_2, Al_2O_3, ZrO_2, ZnO, and TiO_2 P-25 at high temperature which provides insights into gold adsorption and active sites. In situ gold surface plasmon resonance peak shifts from alternating and consecutive adsorption of O_2 to H_2 were correlated to relative charge transfer from/to gold via a Drude-Lorentz model considering contributions from free electrons and interband transitions. A novel methodology matching the relative charge transfer (from O_2 and H_2 adsorption at 398 K and flowing conditions) with Au surface site statistics derived from a truncated octahedron geometric model was used to provide strong in situ experimental and spectroscopic evidence for adsorption of O_2 and H_2 at the gold-support perimeter, which agrees with prior hypotheses for active site location from reactivity and theoretical studies. The prepared catalysts were also evaluated for CO oxidation at 398 K. The resulting TOFs normalized per different surface site location indicated that conversion rates were

not limited by the density of sites at the gold-support perimeter, but by the total gold surface sites, which were also further differentiated by the reducibility of the catalyst support.

Keywords: In Situ UV-Vis Spectroscopy; Gold Catalyst; Surface Plasmon Resonance; Oxygen Adsorption; Hydrogen Adsorption; Site location; Active site; Oxidation; Hydrogenation

1. Introduction

For a long time, gold has attracted the interest of mankind as a valuable metal for use as jewelry and commodity money because of its relatively rareness, malleability, and apparent chemical inertness. Discoveries around the 1980s by Haruta, Hutchings, and others, however, showed that highly dispersed gold is active as a catalyst for several reactions including olefin hydrogenation [1], acetylene hydrochlorination [2], CO [3], olefin [4], and alcohol oxidation [5]. These findings open new possibilities in heterogeneous catalysis, in particular, for highly dispersed gold nanoparticles (NPs) [6]. Among these reactions, oxidation on gold catalysts has been perhaps the most studied for its environmental and industrial relevance in the selective conversion of CO and alcohols and production of propylene oxide and hydrogen peroxide at mild conditions [6]. Due to its optical properties, gold has also found use as a plasmonic sensor in biomedical applications for the determination of kinetics of adsorption of biocompatible chemicals [7] and more recently as a plasmonic catalyst [8]. These applications exploit gold nanoparticles ability to absorb or scatter light in the visible spectrum resulting in strong electromagnetic fields around the nanoparticle [9].

In heterogeneous catalysis, in situ and operando spectroscopic characterizations are required to probe catalysts adsorbed species and active sites at relevant reaction conditions of temperature, pressure, and reactants partial pressures [10]. In combination with kinetic methods, they can be also used to evaluate the kinetic relevance of such surface species in a catalytic cycle [11, 12]. For example, in CO oxidation by gold catalysts, in situ spectroscopic studies have provided a better understanding of intermediate adsorbed species, support oxygen vacancies, gold particle size and oxidation state via Fourier transform infrared (FTIR) [13-15], Raman [15], UV-visible [15], and X-ray absorption spectroscopies (XANES, EXAFS) [16, 17]. Complementary computational and kinetic studies have also helped elucidate the intricacies of CO oxidation mechanism on gold catalysts [6, 13] involving dual active sites (Au and Au-

support interface neighboring sites) or single Au sites only. On Au/TiO_2 catalysts, for example, oxygen active species have been hypothesized to be present along the perimeter of the $Au\text{-}TiO_2$ interface which react with adsorbed CO in a rate controlling step to form CO_2.

In oxidation and hydrogenation reactions, determining adsorption sites of reactants such as O_2 and H_2 can help guide the design of more active catalysts. In the case of O_2 adsorption on gold catalysts, the coverage of such adsorbed O_2 species has been probed with TAP (temporal analysis of products) technique [18, 19]. Other methods such as temperature programmed reduction/oxidation (TPR/TPO) or titration via alternate O_2/CO pulses, but they are limited to reducible supports [20]. The exchange of surface O_2 via $^{18}O/^{16}O$ isotopic exchange on Au/CeO_2 has also been reported, but it requires expensive labeled O_2 [20]. XANES has been also reported to evidence adsorption of O_2 species on Au/TiO_2 [16] and Au/Al_2O_3 [17] during exposure to O_2 and on Au/TiO_2 and Au/TS-1 during in situ transients of propane oxidation with H_2 and O_2 [21-23]. The latter report demonstrated a correlation between Au L_3 XANES whiteline and shifts in the gold plasmon resonance peak as tracked by UV-Vis spectroscopy. These results implied that UV-Vis spectroscopy could be used as a more accessible technique to sense and yield information on species adsorbed on supported polycrystalline gold catalysts. A few reports can be found on the use of plasmon techniques to sense O_2 and H_2 adsorption on gold but mainly on thin films of Au-YSZ (Yttria-stabilized zirconia) [24], $Au\text{-}CeO_2$ [25], $Au\text{-}SiO_2$ [26], $Au\text{-}TiO_2$ [27], and $Au\text{-}ZrO_2$ [27]; and on powder Au/TiO_2 [28, 29]. Recently, the method was exploited to indirectly study heterogeneous catalysts via in situ transmission UV-Vis spectroscopy of thin catalyst coatings deposited over a glass substrate covered with nanofabricated gold disks [30, 31]. Application examples of this method include monitoring adsorbate coverage during CO and H_2 oxidation on Pt nanoparticles [30], NO_x storage kinetics on Pt/BaO [30], oxidation/reduction [31] and H_2 uptake/release in Pd nanoparticles [32]. With the exception of UV-Vis measurements on powder catalysts, all other applications are of limited access, relative expensive, complex, or performed on nanofabricated model thin films. Despite these reports, the application of UV-Vis spectroscopy and gold plasmon resonance to powder catalysts to sense changes in properties relevant to gold catalysis, for example, due to adsorption/desorption of surface species and support properties, has been rarely exploited [21-23, 28, 29].

In this work, we focused on the development of a simple and relatively sensitive in situ gold plasmon UV-Vis spectroscopic methodology to characterize O_2 and H_2 adsorption on gold

nanoparticles supported on a variety of materials including SiO_2, Al_2O_3, ZrO_2, ZnO, and TiO_2 to gain insights into O_2 and H_2 adsorption on surface gold sites. These catalysts were prepared by a deposition-precipitation (DP) method using ammonia as the base titrant rather than the more common sodium hydroxide to avoid sample contamination with Na. SiO_2, Al_2O_3, ZrO_2, ZnO, and TiO_2 materials were chosen because: 1) they are ubiquitous as catalyst supports; 2) they were available in a relatively narrow surface area range ~15-70 m^2/g; and 3) they resulted in samples with gold nanoparticles in the 5-10 nm range and pronounced gold plasmon features. It will be shown that in situ changes of the gold plasmon resonance peak in flowing O_2 or H_2 at high temperature (398 K) can be correlated with adsorption at the metal-support perimeter of the studied gold catalysts. A preliminary evaluation of the catalysts at 398 K in the oxidation of CO will also indicate that at this high temperature, CO conversion rate is not limited by the availability of gold sites at the gold-support interface, but by the overall Au surface atoms. These results highlight the utility of the methodology to study gas adsorption on specific surface sites and its potential for application to in situ/operando spectroscopic and spectrokinetic studies of reactions catalyzed by gold catalysts.

2. Experimental section

2.1.Catalysts preparation

Five different Au catalysts with a nominal metal loading of 1 wt% were prepared by the deposition-precipitation (DP) method using ammonia as the base titrant and commercial metal oxides of intermediate surface area (~15-70 m^2/g): SiO_2 (Grace, Davisil XWP 1000A), Al_2O_3 (Norpro, SA31132), ZnO (Strem Chemicals, 30-1405), (monoclinic) ZrO_2 (Alfa Aesar, 43814), and TiO_2 (P25, Aldrich, 718467). In a typical preparation, 1 g of the support was dispersed in 20 cm^3 of water (Fisher Chemical, HPLC) under stirring (MS-H-Pro Plus hotplate-stirrer, Scilogex). To this stirred slurry, 2.5 wt% NH_4OH (prepared from 14.8 N NH_4OH, Fisher, A669-212) was added dropwise to reach a pH of 9.5 monitored with a DrDAQ pH measuring kit (Pico Technology). After 5 min, about 20 mg of $HAuCl_4.3H_2O$ (Alfa Aesar, 36400) dissolved in 8 cm^3 of water was added dropwise concurrently with 2.5 wt% NH_4OH until the pH was 9.5. In this preparation, NH_4OH was used as a base titrant (instead of the usual NaOH employed in DP) to ensure that all gold was deposited on all supports (including SiO_2) and to avoid catalyst contamination by Na. The solution was then stirred continuously for 1 h after which it was

filtered, washed with abundant water, and dried in vacuum for 12 h at room temperature. The catalysts were treated in static air at 393 K for 2 h (5 K/min) and 673 K for 4 h (4.5 K/min) in a Thermolyne 48000 muffle furnace (Barnstead International). Finally, the calcined catalysts were stored in dark vials and in sealed plastic bags to minimize light and moisture exposure. For comparison with these catalysts, experiments were also performed with an AUROlite^{TM} Au(1 wt%)/TiO_2 (Strem chemicals, 79-0165).

2.2.Catalysts characterization

Fresh and used catalysts were characterized by transmission electron microscopy (TEM) using a FEI Tecnai F20 XT microscope operating at a voltage of 200 kV. The TEM samples were prepared by dispersing the catalysts in ethanol and sonicating the solution for about 10 min. A drop of the dispersed catalyst was then suspended on a 400-mesh copper grid containing ultra-thin carbon film on a lacey carbon support film (P/N 01824, Ted Pella Inc.). Particle size and distribution were calculated for about 50-100 particles from TEM images as counted and analyzed by ImageJ software (https://imagej.nih.gov/ij/). Catalysts and supports were also characterized by N_2 physisorption, X-ray diffraction, and SEM-EDX (**Tables S1-S2, Figures S1-S7**).

2.3.In situ (UV-Vis) gold surface plasmon resonance during O_2/He/H_2 cycles

For the in situ gold plasmon resonance experiments, the catalyst samples were placed in a modified high temperature in situ/operando diffuse reflectance Harrick reaction cell [33]. Originally designed for bench top scanning spectrometers, the cell was modified to enable faster transfer of gases and faster acquisition of in situ UV-Vis spectra. A thorough description of the modifications to the cell (including 3D pdf models and blueprints), its thermal analysis, and its flow dynamics have been reported recently [33]. The UV-Vis light contacting the catalyst originates from a preconfigured dual UV-Vis lamp set up that includes an SL3 Deuterium lamp and an SL1-filter halogen lamp (Stellar Net) through a 600 µm core diameter high-temperature fiber optics probe (Avantes) and which gets reflected back to a Black-comet SR concave grating spectrometer equipped with a CCD detector (Model C, Stellar Net) for analysis. The spectra (1300 ms integration time, 1 scan) were collected over the 230-1080 nm range to enable the characterization of small changes to the gold plasmon resonance peak in real time and in situ on

exposure to different gas atmospheres. To avoid deuterium spikes around 485 nm originating from the lamp, a U-330 filter was used. Prior to the in situ experiments, a given amount of the freshly calcined catalysts (**Table S2**) was loaded to the in situ cell sample cup (~0.15 cm^3) where it was reduced for 30 min at 473 K with pure H_2 at a flow rate of 45 cm^3/min. After reduction, the cell was flushed with helium (45 cm^3/min) and the temperature of the sample was brought down to 398 K (5 K/min). The catalyst sample was then exposed to O_2 (Matheson, UHP, 99.98%) for 30 min at a flow rate of 45 cm^3/min, flushed with helium (Matheson, UHP, 99.999%) for about 15-20 min to purge the lines and cell, and exposed to H_2 for 30 min (45 cm^3/min; Matheson, UHP, 99.999%). This O_2/He/H_2 sequence was repeated several times over 5 h for all the 6 catalysts to ensure the reproducibility of the results. The He purge after O_2 or H_2 contact is used to avoid possible artifacts by the presence of gas phase or weakly adsorbed adsorbates. All gas cylinders are provided with moisture (Matheson, 450B series, type 451: for all gases), oxygen (Perkin Elmer, P/N N9301179: for He, H_2, and CO), and hydrocarbon (Matheson, 450B series, type 454: for He, H_2, and O_2) traps. The collected UV-Vis spectra were referenced to $BaSO_4$ (Sigma Aldrich, P/N 243353) at ambient conditions. It is worth noting that the Au plasmon band has been previously studied in different gas atmospheres for Au/YSZ, Au/TiO_2, and Au/CeO_2 thin films in transmission mode [25, 34]. Here, diffuse reflectance of powder catalysts was used because: 1) it does not require sample preparation; 2) it closely resembles a fixed bed reactor commonly used in heterogeneous catalysis and 3) it has the potential for use in in situ/operando spectroscopic studies.

Lastly, to minimize arbitrary reading errors, the Au plasmon maximum peak positions were automatically determined over the entire duration of the experiments with a homemade Python (www.python.org) computer program by fitting the data ~100 nm around the Au plasmon peak to a polynomial of order 6. The Python program used the *minimize_scalar* and *polyfit* fitting functions available in the NumPy package (www.numpy.org). This procedure resulted in less noisy data when compared to one based on the data's first derivative.

2.4. CO oxidation activity tests

The gold catalysts were also tested for CO oxidation in the modified in situ/operando diffuse reflectance UV-Vis reaction cell. A total gas flow rate of 60 cm^3/min (1 kPa CO, 2 kPa O_2, He balance) at 398 K and 101 kPa total pressure were employed so that a stoichiometric excess of

O_2 was present. CO conversion was measured online by means of an Omnistar GSD 320 O mass spectrometer (MS, Pfeiffer Vacuum) using calibrated gas signals. Conversions were corrected for any CO_2 present in the gas mixture by subtracting baseline signals in a reactor bypass run. CO oxidation conducted on SiO_2 sand (Sigma-Aldrich, P/N 84878) showed negligible conversion demonstrating the inertness of the reaction cell at the studied conditions.

3. Results and discussion

3.1.Catalyst synthesis and characterization

We employed gold nanoparticles deposited on a variety of supports of intermediate surface areas (ZnO, ZrO_2, Al_2O_3, TiO_2, and SiO_2, ~15-70 m^2/g), prepared with the same ammonia deposition-precipitation (NH_3-DP) method which resulted in similar gold loadings (~1 wt%) and close average gold particle diameter (*d*) in the 5-10 nm, while minimizing surface contamination with undesirable Na ion, and resulting in samples with pronounced gold plasmon features. The NH_3-DP method was also tried with a CeO_2 support but failed to produce a catalyst with adequate plasmon characteristics. It is worth noting that the NH_3-DP synthesis method employed in this work carries the risk of forming fulminating gold which is a shock-sensitive and explosive material [35]. We have used this synthesis method for ~1 wt% Au deposition on silicates, titanosilicates, and now on several oxidic supports (SiO_2, Al_2O_3, ZrO_2, ZnO, and TiO_2) without any safety incidents [6, 23, 36, 37].

All catalysts were characterized with N_2 physisorption, X-ray diffraction, scanning electron microscopy-energy dispersive X-ray (SEM-EDX) analysis, transmission electron microscopy (TEM), and in situ UV-Vis spectroscopy. The supports and catalysts textural properties and X-ray diffractograms are reported in **Tables S1 and S2** and **Figure S1**. They show that the supports conserved their integrity after the NH_3-DP method as only small changes were noticed in the textural properties and crystal structure. Except for Au/Al_2O_3 and Au/SiO_2, which showed small peaks due to the presence of Au, all other catalysts lacked any noticeable XRD Au signals suggesting that Au dispersion was relatively high. SEM-EDX analysis of the prepared gold catalysts showed that, except for Al_2O_3 (on which ~80% of the nominal gold was deposited), the NH_3-DP method resulted in Au deposition efficiencies of 95-100% on all supports due to ammonia surface modification (**Figures S2-S7, Table S2**).

TEM images and Au particle size and distribution of the prepared catalysts are shown in **Figure 1**. It was found that, for all supports, the NH_3-DP method enabled gold average particle diameters in the range of 5.5-9.2 nm and with a relative close standard deviation (±1.0-2.0 nm) increasing in the following order: Au/ZnO (d = 5.5±1.0 nm) < Au/ZrO_2 (d = 6.4±1.5 nm) < Au/Al_2O_3 (d = 7.6±1.2 nm) < Au/TiO_2 (d = 7.8±1.6 nm) < Au/SiO_2 (d = 9.2±2.0 nm). TEM images of used gold catalysts shown in **Figure S8** also indicate that the average Au particle size only suffers minimum changes after exposure to flowing O_2 and H_2 at reaction conditions for the duration of the experiments; therefore, for simplicity, only average particle sizes of the freshly calcined catalysts will be used for subsequent discussion.

The in situ diffuse reflectance UV-Vis spectra of the supported gold catalysts in flowing O_2 and H_2 at 398 K in **Figure S9** show that the Au plasmon peak is symmetric for Au/SiO_2, Au/Al_2O_3, and Au/ZrO_2. Such symmetry is characteristic of Au NPs with regular morphology and with a relatively narrow size distribution in agreement with the results in **Figure 1** [38]. In the case of Au/ZnO and Au/TiO_2 the Au plasmon band appeared slightly broadened to higher wavelengths. This could be assigned to a stronger interaction between Au NPs and reducible supports. A small broadening of the Au plasmon band during exposure to O_2 appears to be related to charge transfer to gold and a slight flattening of the gold NPs as proposed by Borensztein et al. [28] Lastly, **Figure S10** shows TiO_2 P25, an example of a support, under similar in situ UV-Vis in O_2 and H_2 environments as that for the gold catalysts confirming the absence of any support spectral shifts in the Au plasmon region. It is worth noting that the Au particle size obtained in the prepared catalysts via ammonia-DP is relatively larger than those prepared by the more common DP method using NaOH as the basic titrant. However, these larger Au NP sizes are not unusual and have been previously reported with the NH_3-DP synthesis method and on SiO_2 yielding Au NPs in the 2-16 nm range, whose final size value depended on the synthesis pH, temperature, and reaction time [39, 40]. At present, it is unclear why the NH_3-DP method leads to larger nanoparticles in Au/TiO_2 *vs* the Au/TiO_2 (commercial), but a possible reason may be the different preparation conditions: NH_3-DP at pH=9 *vs* NaOH-DP at pH~7 (Haruta's original DP method [4]) which was more likely used for the commercial Au/TiO_2 sample. These two experimental conditions can result in different Au species and Na and Cl content on the prepared sample, which are known to affect particle size growth and sintering [6, 41].

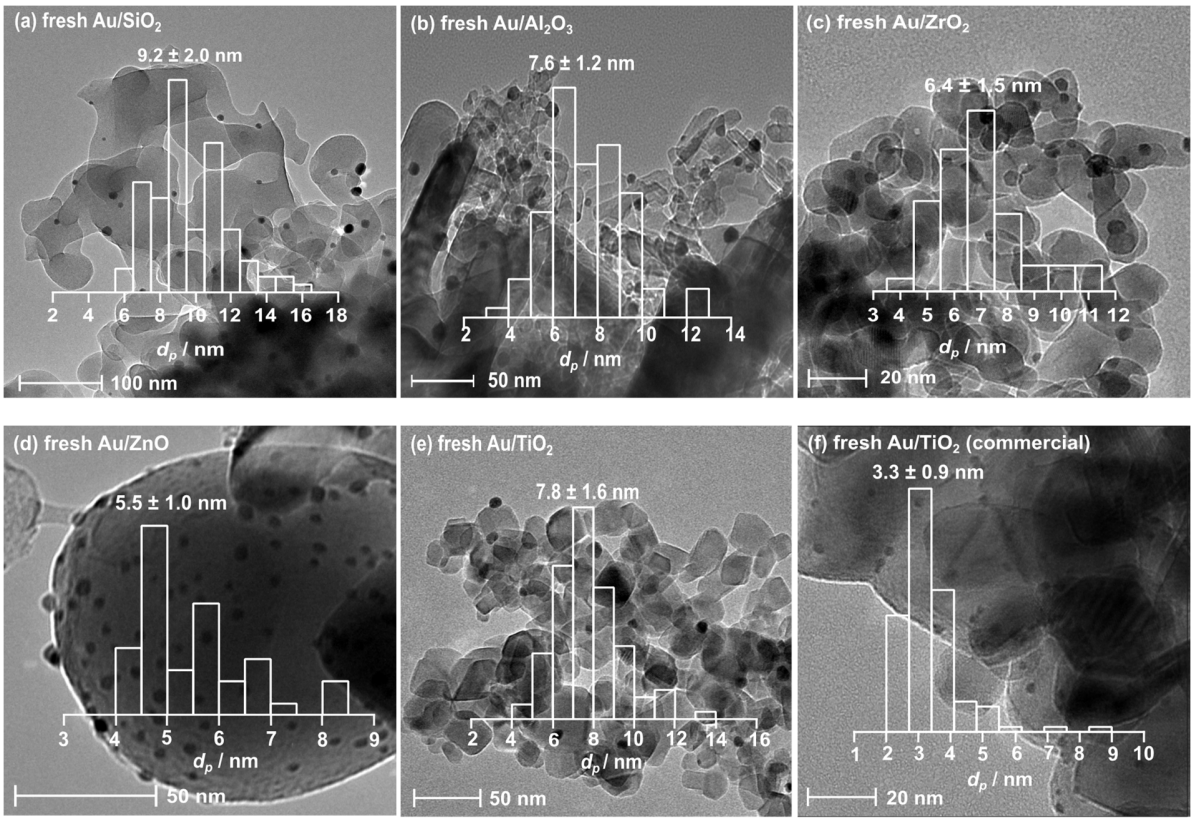

Figure 1. TEM images of calcined Au catalysts: Au/SiO_2, b) Au/Al_2O_3, c) Au/ZrO_2, d) Au/ZnO, e) Au/TiO_2, and f) Au/TiO_2 (commercial). Approximately 50-100 particles were counted to obtain the particle size distributions.

The TEM images in **Figure 1** show that Au NPs are quasi spherical. Because of the average diameter of the Au NPs in the 5.5-9 nm range, they are more likely to be described reasonably well by a truncated octahedron. Such structure has been previously reported from high resolution TEM characterization on Au/TiO_2 (d=1.5-4.8 nm) [42] and Au/Fe_2O_3 (d=2.2-3.5 nm) [43], however, the truncated cuboctahedron has also been observed for Au/TiO_2 (d~2-4 nm) [44] and Au/Al_2O_3 (d~2-4 nm) [44] catalysts. More recent ETEM studies on Au/TiO_2 (d=3-4 nm) [45] and Au/CeO_2 (d~3-4 nm) [46] in O_2 and CO atmospheres also reported structures that resemble a truncated octahedral geometry. Based on DFT calculations, this geometry has been found to be the most energetically favored for Au NPs above 2-3 nm diameters [47], whereas the cuboctahedron structure was found to be the most stable for Au NPs below 1 nm [48]. Overall,

the Au NPs of the catalysts in this work can thus be fairly modeled as a truncated octahedron for Au site statistics purposes, which will be discussed in the following sections, whereas a truncated cuboctahedron geometry will be used for comparison.

3.2.Relationship between surface plasmon resonance peak position changes and relative charge transfer to/from Au nanoparticles

In order to relate gas adsorption to Au surface sites, the change in the Au plasmon peak position needs to be related to physicochemical changes during adsorption. Here, we relate Au plasmon peak shifts to changes in charge transfer to/from Au nanoparticles occurring during gas adsorption. In order to do so, we chose a simple model that is able to explain moderately well the optical properties of supported Au nanoparticles in the proximity of the plasmon peak. In diffuse reflectance measurements such as those in the present study, the Shuster-Kubelka-Munk theory relates the absolute reflectance (R_∞) to the ratio of absorption (K) and scattering (S) coefficients via the commonly called Kubelka-Munk function in Eq. 1 [49]:

$$F(R_\infty) = \left[\frac{(1-R_\infty)^2}{2R_\infty}\right] = \frac{K}{S} \qquad \text{Eq. 1}$$

Where R_∞ is taken as the ratio of the light intensity reflected from the catalyst sample to that of $BaSO_4$, the white reference. In the present experiments, the catalyst sieved particle sizes were within 38-75 μm. At these conditions, the scattering coefficient (S) (dominated by support scattering because of the significantly larger support grain *vs* Au NPs size) is considered to be independent of wavelength, thus the Kubelka-Munk function is primarily a function of the absorption coefficient *K* [28, 49, 50]. Since the visible range absorption from the oxide supports is significantly smaller than that for Au nanoparticles, the main contributions to *K* arise from Au nanoparticles absorption, $K = 2N_{Au}C_{abs}$, where N_{Au} is the number of Au nanoparticles per unit volume and C_{abs} is the absorption cross-section [28, 51]. If we take a model of absorption by small nanospheroids with semi-axes *a*, *b*, and *c* and an average particle radius much smaller than the photon wavelength (r << λ), then C_{abs} can be given as a function of the dielectric function of the nanospheroids, $\epsilon = \epsilon_1 + i\epsilon_2$, by Eq. 2 [9, 51]:

$$C_{abs} = \frac{2\pi\epsilon_m^{1/2}}{\lambda} Im\{\alpha\} \qquad \text{Eq. 2}$$

Where, ϵ_m is the dielectric function of the surrounding medium; for a supported Au nanoparticle, ϵ_m it is taken approximately as an averaged dielectric function between the gas environment and that of the support material [9] and α is the polarizability of the Au nanoparticle given by Eq. 3 [51]:

$$\alpha = \frac{4}{3}\pi abc\ \frac{\epsilon - \epsilon_m}{\epsilon_m + L(\epsilon - \epsilon_m)} \qquad \text{Eq. 3}$$

Solving Eqs. 2 and 3 gives:

$$C_{abs} = \frac{24\pi^2 abc\ \epsilon_m^{3/2}}{\lambda} \frac{\epsilon_2}{[L\epsilon_1 + (1-L)\epsilon_m]^2 + (L\epsilon_2)^2} \qquad \text{Eq. 4}$$

Where ϵ_1 and ϵ_2 are the real and imaginary parts of the dielectric function of the Au nanoparticle, and L is a nanoparticle geometrical factor (e.g., for a sphere $a = b = c$ and $L = 1/3$).

Since both free (intraband) and bound (interband) electrons contribute to the dielectric function, intraband (ϵ_f) and interband (ϵ_b) contributions are accounted for by a Drude-Lorentz model with one interband transition (e.g., the fundamental oscillator) [51]. Such model has been shown to fit moderately well the experimentally determined Au dielectric function (ϵ) at wavelengths above 500 nm [52]. Thus, the dielectric function wan be represented by Eqs 5-7:

$$\epsilon = \epsilon_f + \epsilon_b \qquad \text{Eq. 5}$$

$$\epsilon_f = \epsilon_\infty - \frac{\omega_p^2}{\omega^2 + i\omega\gamma_f} \qquad \text{Eq. 6}$$

$$\epsilon_b = \frac{\omega_p^2}{\omega_0^2 - \omega^2 + i\omega\gamma_b} \qquad \text{Eq. 7}$$

Where ϵ_∞ is an offset constant when working at wavelengths longer than the resonance wavelength [*52*], ω is the impinging wave frequency ($\omega = 2\pi c/\lambda$), ω_p is the plasma frequency of the bulk Au ($\omega_p^2 = Ne^2/m\varepsilon_0$; N is the conduction electron density, e and m are the charge and mass of the electron, respectively, and ε_0 is the permittivity of vacuum), ω_0 is the oscillation frequency of a bound electron under an electric field, and γ_f and γ_b are damping constants for free and bound electrons, respectively. For ω near $\omega_{max} \approx \omega_0$ and for $\omega \gg \gamma$ [*51*, *53*] then:

$$\epsilon_1 = \epsilon^{\infty} - \frac{\omega_p^2}{\omega^2} f_1(\omega) \quad \text{Eq. 8}$$

$$\epsilon_2 = \frac{\omega_p^2 \gamma_f}{\omega^3} f_2(\omega) \quad \text{Eq. 9}$$

Where,

$$f_1(\omega) = 1 - \frac{1}{2\omega_0} \frac{\omega^2(\omega_0 - \omega)}{(\omega_0 - \omega)^2 + (\gamma_b/2)^2} \quad \text{Eq.10}$$

$$f_2(\omega) = 1 + \frac{1}{4\omega_0} \frac{\omega^3}{(\omega_0 - \omega)^2 + (\gamma_b/2)^2} \quad \text{Eq.11}$$

Thus, the plasmon peak position can be found from the maximum of C_{abs}, which from Eqs. 2 and 3 occurs when:

$$\epsilon_{\mathrm{m}} + L(\epsilon - \epsilon_m) = 0 \quad \text{Eq.12}$$

If charge transfer occurs on Au from gas adsorption and is reflected as a change in the conduction electron density (ΔN), the shifted plasmon frequency position is obtained by replacing N with $N + \Delta N$ in the expression for ω_p and along with Eqs. 5-12 results in [*53-55*]:

$$\frac{\Delta N}{N} = \frac{\lambda_m^2}{\lambda^2} - 1 \quad \text{Eq. 13}$$

Where $\Delta N/N$ is the relative change in charge transfer on Au, λ_m is the wavelength at which maximum absorption occurs corresponding to the initial reference charge density N, and λ is the shifted wavelength maximum after charge transfer.

3.3.In situ Au surface plasmon resonance during O_2, He, and H_2 exposure

Resonant oscillations occur on a metal surface typically due to interaction with visible light. These localized oscillations near metal nanoparticles (NPs), known as localized surface plasmon resonance [31], result in a strongly enhanced electromagnetic field around the nanoparticle and which for Au NPs manifest themselves as a broad band that falls in the visible region of the electromagnetic spectrum. The peak position of the Au plasmon band is sensitive to changes at the boundary of the metal nanoparticle and its surrounding medium [9], which makes it an

efficient tool for obtaining information on physicochemical properties around the gold NPs. Here, the changes in Au plasmon peak position of supported gold nanoparticles were monitored in real time with a modified in situ diffuse reflectance UV-Vis spectroscopic cell under oxidizing and reducing conditions [33].

The in situ diffuse reflectance UV-Vis spectra of the catalysts were measured in flowing O_2 and H_2 atmospheres at 398 K. **Figure 2** shows a typical pseudo-absorbance *vs* wavelength spectra for the Au/TiO_2 catalyst. A peak centered around 570 nm and generally broad between 500 and 650 nm corresponded to Au plasmon. When the catalyst was exposed to O_2 the peak position was centered around 575 nm, whereas in H_2, the Au plasmon position shifted to about 565 nm. This blue shift can be explained as a result of charge transfer from hydrogen to Au [56]. Such shift is expected from an increase in the conduction electron density as noted from analysis of Eq. 13 [9, 54].

Eq. 13 is a simplified view of the Au plasmon phenomenon as it only reflects properties over a limited range of experimental conditions in the proximity of the Au plasmon peak; nevertheless, it still describes in a relatively simple manner the relationship between the Au plasmon peak position and charge transfer (ΔN) sufficient enough to capture adsorption events as a result of titration of O_2 with H_2 or H_2 with O_2. The observed increase in the energy of the peak position (blue shift) upon O_2 titration with H_2 is in concordance with experimental and modelling results of the plasmon process on gold catalysts when exposed to reducing environments showing the preponderance of electron charge transfer to or from the gold nanoparticles [28, 56]. These effects are also evident from DFT calculations showing a weakening of the O-O bond during O_2 adsorption on $Au/TiO_2(101)$ as a result of charge transfer from Au to O_2 antibonding orbitals [57], and from theoretical calculations which showed electrochemical charge transfer from Au NPs to diffusing oxygen ions in a Au-YSZ thin film [24]. In the case of H_2 adsorption on Au, theoretical [58] and experimental evidence via Au plasmon on Au/YSZ nanocomposites [34] and Au/Pt nanoparticles embedded in ZnO and TiO_2 [56] showed that adsorbed H_2 transfers charge to Au, resulting in a blue shift (lower wavelength or higher energy) as seen in **Figures 2** and **3**. In summary, the Au plasmon peak position is sensitive to adsorption of oxidizing or reducing molecules as manifested by peak shifts determined in the studied catalysts to be primarily due to charge transfer events. This phenomenon is exploited here to track the

adsorption of O_2 or H_2 on gold catalysts at reaction conditions from Au plasmon peak position shifts as measured via in situ UV-Vis spectroscopy.

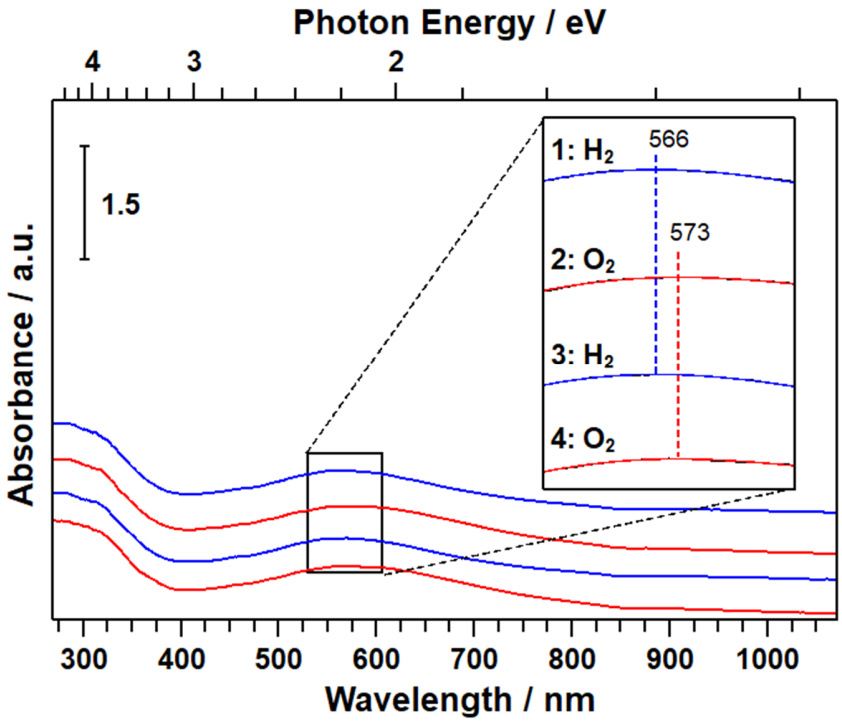

Figure 2. Typical in situ diffuse reflectance UV-Vis spectra of Au/TiO_2 catalyst upon exposure to flowing H_2 and O_2 at 398 K. Numbers indicate the measurement sequence. He was used to flush gases in between H_2 and O_2 cycles, spectra in He were slightly smaller to those of the prior gas and not shown for simplicity (Au plasmon peak positions in O_2, H_2, and He are shown in **Table S3**). The inset shows more clearly the peak maximum for the different traces obtained via an automated procedure (by fitting the data around the maximum to a polynomial function of order 6).

Figure 3 shows the change in Au plasmon peak position on all gold catalysts (Au/SiO_2, Au/Al_2O_3, Au/ZrO_2, Au/ZnO, Au/TiO_2, and Au/TiO_2-commercial) as a function of exposure time to alternating O_2, He, H_2, and He gases for 5 h (average and standard deviation of Au plasmon peaks is presented in **Table S3**). Several qualitative observations can be made:

1) The shift of the Au plasmon peak between oxidizing and reducing atmospheres or vice versa was completely reversible and reproducible, indicating minimum irreversible changes to catalyst properties and gold average particle size as a result of gas exposure

[59]. This is evidenced by the similarity between average particle sizes of fresh and used catalysts (**Figure S8**).

2) For all catalysts, the Au plasmon peak position shifted towards higher wavelengths (lower energies) on exposure to O_2, decreased slightly in He flow as a result of partial desorption of adsorbed O_2, and decreased significantly on exposure to H_2 (the opposite was also true when switching from H_2 to O_2 gas). The relative change in Au plasmon peak position ($\Delta\lambda$) in going from either O_2 to H_2 or H_2 to O_2 exposure was almost identical and increased in the following order: $\Delta\lambda$ Au/SiO_2 ~ 2 nm < Au/Al_2O_3 ~ 4 nm < Au/ZrO_2 ~ 6 nm < Au/TiO_2 ~ 9 nm < Au/ZnO ~ 11 nm > Au/TiO_2-commercial ~ 23 nm.

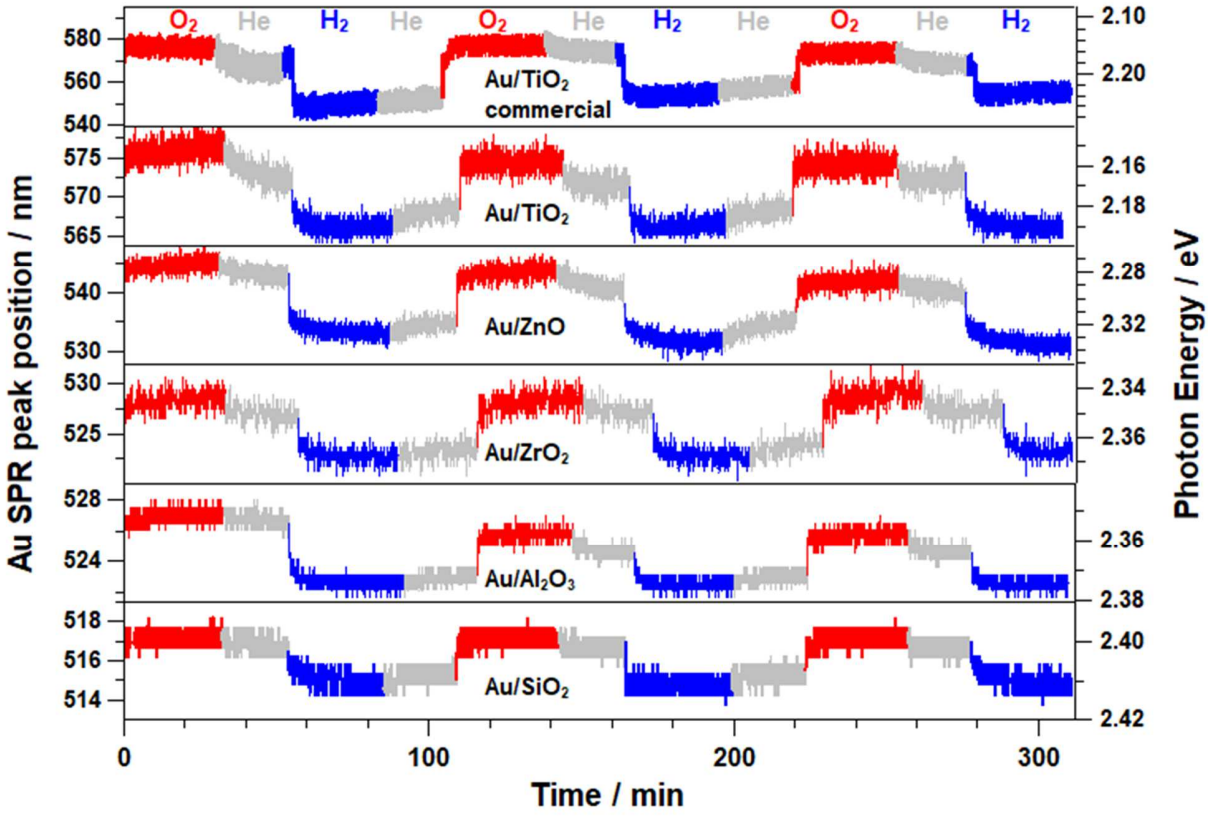

Figure 3. Supported gold catalysts characterization by Au plasmon peak position changes as determined from in situ UV-Vis spectroscopy after catalysts exposure to alternating flowing H_2 and O_2 at 398 K.

The observed Au plasmon peak shifts when catalysts were exposed to O_2 or H_2 are ascribed to O_2 and H_2 adsorption, respectively. When O_2 or H_2 exposed catalysts were subsequently treated with H_2 or O_2, respectively, they initially react to form water until the former adsorbed gas is fully consumed, this is expected since gold nanoparticles are well known H_2 oxidation catalysts. It is widely recognized that clean gold surfaces are not favorable for O_2 adsorption, but that the presence of coordinatively unsaturated sites due to special gold geometry, the presence of a metal-gold interface as that present in supported catalysts, or the presence of coadsorbates significantly favors O_2 or H_2 adsorption [60, 61]. O_2 chemisorption on Au nanoparticles has been reported for Au/TiO_2 and Au/Al_2O_3 exposed to O_2 as followed by in situ Au L3 XANES. In these reports, the formation of Au-O species was inferred by an increase in the intensity of the XANES white line due to the decrease of the electron count in the d orbital of Au as they transferred to the $2\pi^*$ orbital of O_2 [17, 22, 23]. This charge transfer from Au to O_2 was also evidenced by in situ XANES and a red shift of the Au plasmon by in situ UV-Vis spectroscopy during propane partial oxidation on Au/TiO_2 and Au/TS-1 [22, 23]. While Au plasmon position appears to be quite sensitive to charge transfer due to O_2 chemisorption, the nature of the Au-O adsorbed species is still unclear because XANES and UV-Vis spectroscopies cannot discriminate among O_2, O^-, O_2^-, O^{2-}, hydroxyls, or hydroperoxo species which could form on Au or at the Au-support perimeter during O_2 chemisorption or after reaction with H_2 [22, 23]. Further experiments, for example, based on in situ EPR [36] or kinetic measurements for O_2 reaction order dependence [62] followed by in situ Au plasmon during oxidation reactions could also provide more clarity on the nature of these species.

Upon exposure to O_2, there is the possibility that Au in the catalysts of **Figure 3** become oxidized. However, this is less unlikely on these catalysts because of the relatively large Au NPs sizes which are more difficult to oxidize than Au NPs smaller than 3 nm [28, 63]. This is supported by previous in situ Au L3 XANES and UV-Vis spectroscopic characterization of Au/TiO_2 and Au/TS-1 during propane oxidation with H_2 and O_2 [21-23] which showed that Au remained in a metallic state upon O_2 adsorption. Similar findings were also reported by Bokhoven et al. from in situ Au L3 XANES on Au/TiO_2 and Au/Al_2O_3 (d~1-3 nm Au NPs) when exposed to CO/O_2 mixtures [16, 17]. Theoretical modelling of metal and support effects on Au/TiO_2 exposed to O_2 by Borensztein et al. [28] considered the formation of a Au NP oxide overlayer and adsorption of O_2 on TiO_2 support. These authors predicted changes to the Au

plasmon peak as a result of a reduction of the metallic Au NP volume (lower intensity), flattening of the Au NP (red shift), presence of a dielectric oxide layer (red shift and damping of the Au plasmon), and changes to the dielectric function of the support (lower intensity). However, these effects on the Au plasmon peak could not fit the experimental observations, which were better explained by charge transfer between Au and O_2 and a small flattening of the Au NPs rather than by a change in the oxidation state of Au or O_2 adsorption on TiO_2. The relatively small Au plasmon peak changes observed for the gold catalysts on this work upon exposure to O_2 (**Figure S9**), further suggest that O_2 species predominantly adsorb on Au or its vicinity, but not as an overlayer oxide, and that Au is more likely to be in a metallic state. Additionally, any effect on the Au plasmon peak due to adsorption of O_2 or H_2 on the supports reported here (**Figure S10**), which are less reducible than TiO_2, should be negligible.

3.4.Consequences of O_2/H_2 adsorption on gold surface plasmon peak position and assessment of gas adsorption sites on gold catalysts

Figure 3 showed that the Au plasmon position is sensitive to switches in the gas environment from O_2 to H_2 (and vice versa) and that it shifts to lower wavelengths due to charge transfer from H_2 to Au as a result of reaction of adsorbed O_2 with H_2 and adsorption of H_2. This process resembles a method reported by Benson and Boudart for Pt catalysts which titrates adsorbed O_2 with H_2 [64], and is typically used for estimation of noble metal dispersion in supported catalysts. On gold catalysts, O_2 titration with H_2 was used for the estimation of gold dispersion on Au/Al_2O_3. However, the method proved to be difficult due to the relatively small amounts of O_2 chemisorbed (<15 μmol/g) that need to be detected, the high dependence on catalyst pretreatment and titration temperature, and the requirements of relatively large amounts of catalyst (0.25-1.0 g) and high reduction pretreatment temperature (>673 K) [65]. This report showed a close agreement between Au particle diameters measured by O_2 titration with H_2 and by TEM, which would seem reasonable if O_2 adsorbed on all surface atoms; however, it is likely that the above complications made this chemisorption method report unreliable as O_2 adsorption on gold catalysts is expected to occur in only a fraction of the Au surface atoms (e.g., at undercoordinated Au sites). In this section, Au plasmon peak position changes will be used to probe such expectations for O_2 and H_2 adsorption on gold catalysts.

The largest changes in Au plasmon peak position in **Figure 3** from O_2 to H_2 (or from H_2 to O_2) gas switches on the studied Au catalysts were found for Au/ZnO ($\Delta\lambda$ = 11 nm, $-\Delta N/N$=4.2%, d = 5.5 nm) and Au/TiO_2 ($\Delta\lambda$ = 9 nm, $-\Delta N/N$=2.9%, d = 7.8 nm) supported catalysts. This is in line with prior reports indicating that oxygen adsorption is more favorable on gold or at the gold-support perimeter of reducible supports [18-20]. The larger shift for Au/ZnO with respect to Au/TiO_2 (both supports are reducible) would at first be unexpected as TiO_2 is a more reducible support than ZnO. However, these results are consistent with a larger adsorption of O_2 or H_2 (i.e., charge transfer) on the Au/ZnO catalyst. This points to a larger gold surface or gold-support perimeter on Au/ZnO than that on Au/TiO_2 that is available for O_2 or H_2 adsorption as a result of a smaller average Au NP size on Au/ZnO ($d \approx 5.5$ nm) *vs* that on Au/TiO_2 ($d \approx 7.8$ nm). This explanation was further confirmed by testing a Au/TiO_2-commercial ($d \approx 3.3$ nm) with smaller particle size, which resulted in a significantly larger Au plasmon peak shift of $\Delta\lambda$ = 23 nm ($-\Delta N/N$=7.8%,) than the Au/TiO_2 ($\Delta\lambda$ = 9 nm, $d \approx 7.8$ nm), confirming a higher gas adsorption on the commercial catalyst because of its larger Au surface sites density including those at the Au-TiO_2 metal-support perimeter. This result clearly shows that the Au plasmon peak changes are sensitive to differences in O_2 and H_2 adsorption even in similar supported catalysts.

Up to now there is no in situ/operando spectroscopic reports on O_2 or H_2 adsorption site location on gold catalysts. Generally, this has been inferred from activity studies of gold catalysts, because specific gold sites (e.g., at the metal-support perimeter) have been typically linked to activation of reactants in various oxidation reactions and thus to high catalytic activity. Of great interest is the hypothesis that gold sites at the metal-support perimeter are involved in oxidation and other reactions as suggested by Haruta more than 20 years ago [66] and evidenced from catalytic reactivity and theoretical calculations [6]. In CO oxidation, for instance, Yates and co-workers [14] and Chandler and co-workers [13] (based on DFT calculations on Au/TiO_2) surmised that CO oxidation occurs at the Au-TiO_2 perimeter. Similarly, Behm and co-workers (based on TAP reactor measurements) also offered kinetic evidenced for the catalytic relevance of the Au-support perimeter for CO oxidation [19]. In the water gas shift reaction, Ribeiro and co-workers also offered kinetic evidence for the importance of gold undercoordinated (corner) atoms at the gold-support interface [67]. Based on all these prior works, it is reasonable to expect that gold-support perimeter sites play a significant role for oxygen adsorption in reactions such

as CO oxidation. In summary, if the adsorption of O_2 (or H_2) on Au catalysts occurs predominantly on the same type of Au sites, namely Au-support perimeter, then, altogether these results and theoretical calculations predict a correlation between the relative charge transfer change which can be estimated here from $\Delta N/N$ in Eq. 13 as a result of O_2 (or H_2) adsorption on Au surface sites and the fraction of Au-support perimeter sites (which can be estimated from geometric models) regardless of the type of support.

To test the assertion that O_2 and H_2 adsorption on Au NPs occurs at the Au-support perimeter regardless of the nature of the support, we studied: 1) the relative change of electron density, $\Delta N/N$, in the gold NPs of various supported gold catalysts resulting from switching flowing O_2 to a H_2 (or H_2 to O_2) gas environment in combination with 2) Au site statistics for top and perimeter sites of various coordination numbers (i.e., corner, edge, face) as a function of Au NP diameter, d. These site correlations of top and perimeter Au atoms in a NP for particle diameters in the 1.7-14 nm range were determined from the geometry of the top slice of a truncated octahedron [68]. For comparison, the site statistics of a truncated cuboctahedron were also evaluated [67]. A detailed description of the Au sites, count, and formulas is given in **Tables S4-S7** and **Figure S11**. Despite the limited number of catalysts studied in this work, the observed relationship between the average particle diameter (d) and gold atom sites allowed us to assess the site location for adsorption of O_2 and H_2 on the studied gold catalysts. More specifically, it is expected that experimental in situ UV-Vis spectroscopic data for the tested catalysts' electron charge change, $\Delta N/N$, would track with specific sites and therefore allow us to determine the location of O_2 and H_2 adsorption on the supported gold catalysts.

Figure 4 presents a plot of Au particle diameter for the studied catalysts alongside with 1) Au site dispersion (D) statistics of top and perimeter (corner, edge, face) atoms based on truncated octahedron (solid lines) and cuboctahedron (dashed lines) Au nanoparticle models and 2) relative charge transfer (CT) change ($\Delta N/N$) calculated from in situ Au plasmon peak position changes in going from flowing O_2 to H_2 (or H_2 to O_2) (solid squares) or after flushing with He (empty squares) at 398 K. Since the Au plasmon peak change was almost identical in **Figure 3** in going from O_2 to H_2 or from H_2 to O_2, only the former changes were plotted in **Figure 4**. It is clear from **Figure 4** that a trend exists between the CT (due to H_2 or O_2 adsorption in flow conditions) and the dispersion of Au perimeter sites (solid squares). A similar trend, but with slightly lower $\Delta N/N$ values, is also observed for $\Delta N/N$ calculated with Au plasmon peak positions after flushing

gas phase H_2 or O_2 with He (empty squares) to remove loosely adsorbed species. Judging from the slightly higher CT change in flowing H_2 or O_2, it appears that some of the O_2 or H_2 species are weakly adsorbed on undercoordinated (CN = 6, 7) top sites of the Au NP, but which are flushed in He flow (**Table S3**). This indicates that the majority of the O_2 or H_2 species remains strongly adsorbed at the Au-support perimeter. These results clearly indicate that O_2 and H_2 species remain strongly adsorbed on undercoordinated Au sites (CN = 5, 6, 7) predominantly located at the Au-support perimeter.

While the site statistics in **Figure 4** are based on Au NPs with a truncated octahedron geometry (solid lines), it is also clear that the above conclusions are also valid for Au NPs of truncated cuboctahedron geometry (dashed lines), that O_2 and H_2 species adsorb at the Au-support perimeter. In the case of O_2 species adsorption on supported Au nanoparticles, the in situ experimental results in **Figure 4** agree with prior expectations and theoretical and experimental kinetic and reactivity studies that suggested that O_2 species adsorb at the boundary region between Au and the support metal oxide where they can then be removed with low energy barriers via oxidation reactions [6, 13, 14, 19, 69, 70]. These results are remarkable as they represent the first in situ UV-Vis spectroscopic evidence at relevant reaction conditions of O_2 and H_2 species adsorption at the metal-support perimeter [71]. They confirm, at least at the evaluated conditions, the relevance of a small number of Au surface sites (<10%) for O_2 and H_2 adsorption and also likely for related oxidation and hydrogenation reactions. They also show a close relationship between the same active sites in O_2 and H_2 adsorption and H_2 oxidation with O_2 on supported gold catalysts. Such synergy is further supported by DFT calculations on Au/TiO_2 indicating that H_2 oxidation with O_2 is facilitated by H_2 activation on adsorbed O_2 [61, 72] or O_2 activation on adsorbed H_2 [60] at the Au-support perimeter sites where it is dissociated with low activation barriers. This region, the metal-support perimeter, has thus been invoked as the primary reaction zone for H_2 oxidation with adsorbed O_2 on Au/TiO_2 and Au/Al_2O_3 catalysts and these prior assumptions are justified by the present findings [72, 73].

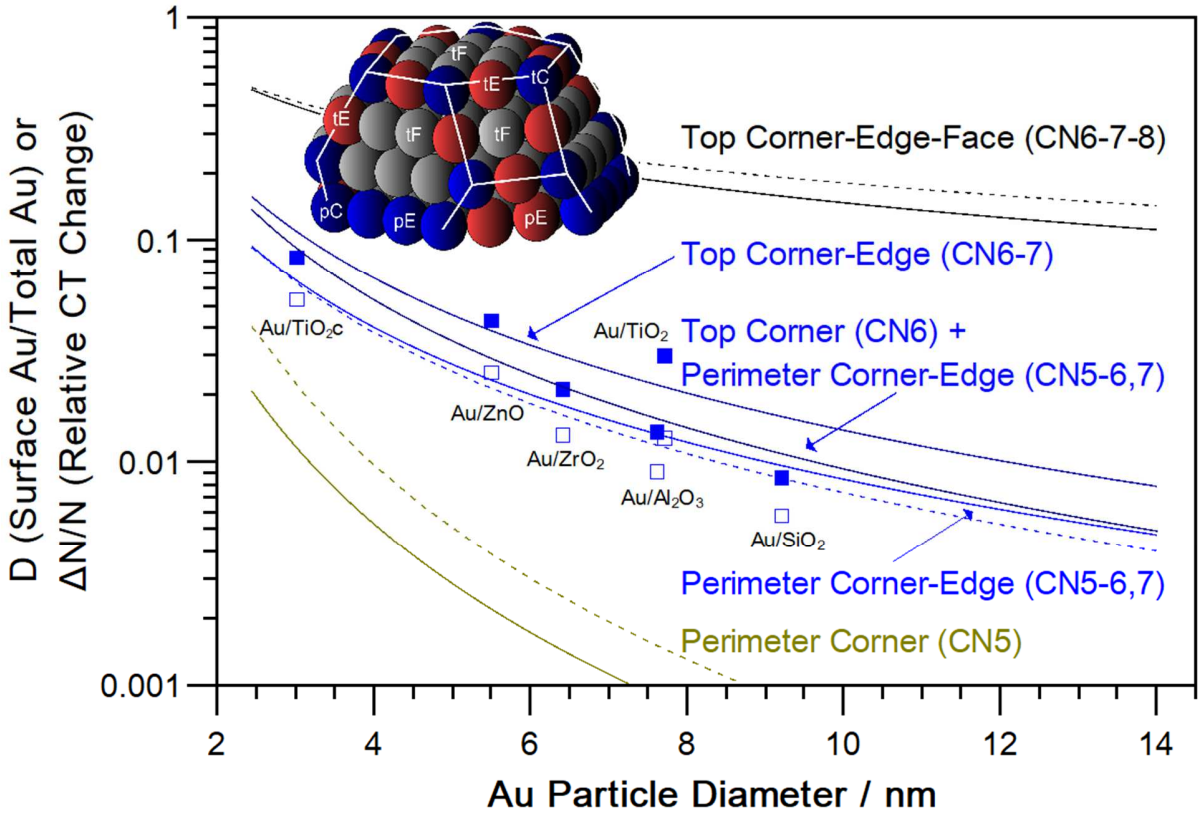

Figure 4. Plot of gold particle diameter (*d*) *vs* dispersion (D) and Δ*N/N* on gold catalysts at 398 K. D defined as the fraction of surface gold atoms with respect to the total Au atoms in a NP (calculated from site statistics for a Au NP with truncated octahedron geometry including atoms coordination number [68], see **Tables S4-S7**), Δ*N/N* is the fraction of electron density change (charge transfer, CT) from Au plasmon shift (Eq. 13, **Table S3**) in flowing O_2 and H_2 (blue solid squares) or in O_2 and H_2 but after flushing with He (blue empty squares). For comparison, the corresponding site statistics for top surface ($0.90d^{-0.70}$), perimeter corner and edge ($0.90d^{-1.8}$), and perimeter corner ($0.90d^{-2.9}$) atoms for a truncated cuboctahedron geometry are also presented (dotted line) [67].

O_2 adsorption at the Au-support interface has been widely speculated and evidenced from non-spectroscopic methods. This has also been the case for the related H_2 adsorption [6, 66, 71]. For example, Haruta and co-workers demonstrated via H_2-D_2 exchange that H_2 dissociation occurred at the perimeter interface of Au/TiO_2(110) surfaces containing Au nanoparticles of different sizes and at temperatures between 350-450 K [74]. The relevance of these periphery

sites for D_2 and H_2 adsorption was also supported by recent DFT calculations for Au/TiO_2 [61]. DFT calculations also showed that O_2 adsorption and activation is greatly facilitated by the presence of dissociatively adsorbed hydrogen at undercoordinated Au sites [60]. Overall, the in situ UV-Vis spectroscopic results in this work supported by prior kinetic and DFT calculations clearly evidence H_2 and O_2 adsorption and their synergy for oxidation reactions at the Au metal-support perimeter. However, the nature of the surface species and the fundamental surface mechanism by which this synergy operates remain unknown as UV-Vis spectroscopic results alone cannot discriminate among different adsorbed species (i.e., OH, OOH, O_2^-, O^-, O^{2-}, etc) and their relevance as intermediates in oxidation or hydrogenation reactions; thus, further work is granted with in situ/operando spectroscopy, theory and kinetics to further elucidate such mechanistic inquiries. Other spectroscopic techniques could be suggested for characterization of these adsorbed species, for example, by EPR to probe the possible presence of oxygen radical species [75], by FTIR to monitor H_2 adsorption [76], trapped H in the support conduction band edge, OH or H_2O [14, 72], and by AP-XPS to track O species. However, these techniques often times require low temperatures and pressures far away from typical catalyzed reaction conditions, can result in flawed conclusions as in the case of AP-XPS where X-rays can lead to Au oxidation [77], and cannot discriminate the location of the adsorption sites. Clearly, new in situ spectroscopic methodologies are needed to gain access to the nature and activity of adsorbed species at the gold-support perimeter interface [78]. These challenges of characterizing H_2 and O_2 species adsorbed on Au catalysts further emphasize the novelty and deceiving simplicity of the present spectroscopic approach and findings for gold catalysis as it is performed with a commonly available and affordable UV-Vis technique, on powder polycrystalline catalysts, at reaction conditions, and with the ability to probe the near vicinity of supported gold nanoparticles.

3.5.Implications for catalysis on supported gold catalysts

The in situ spectroscopic findings in this work that the support-perimeter interface sites in gold catalysts are the predominant adsorption location for O_2 and H_2 species provide needed experimental evidence and a methodology to address additional unresolved questions in catalysis by supported gold nanoparticles. Of particular interest are questions regarding the contributions to catalytic activity by support interactions with Au and adsorbed species. As an example, we

consider CO oxidation on gold catalysts, which has been studied extensively, but whose mechanism is still a matter of debate. The reasons for this arise from the wide variety of conditions tested including differences in:

a) Reaction conditions: possibly leading to different kinetic dependences, for example, low *vs* high temperature mechanisms [19, 79, 80].
b) Au particle size and morphology: resulting in different distribution of site coordination, for instance, corner [70, 81], surface [79], and perimeter atoms [6, 66, 81], whose role in adsorption and catalytic properties may be different.
c) Support nature: for example, reducible *vs* nonreducible [18, 82], which can affect the presence or absence of oxygen vacancies [69] and bulk defects [83].
d) Presence or absence of water [13, 84], which can promote catalytic activity by formation of active hydroperoxide species or block active sites.
e) Carbonate poisoning [84-86], which could reduce catalytic performance in an otherwise active catalyst.
f) Presence of impurities, which can lead to detrimental catalytic activity [87].

With regards to support effects, for example, there are varied hypotheses to explain activity differences, perhaps due to the difficulty in decoupling all of the above variables and the lack of systematic studies. To highlight these points and the utility of the spectroscopic methodology developed in this work, preliminary activity results are presented for CO oxidation with the prepared catalysts at the same reaction conditions (temperature of 398 K matching that of the spectroscopic study, total pressure of 101 kPa, 1 kPa CO, 2 kPa O_2, and He balance, no co-fed water), prepared with the same NH_3-DP (no residual Na) method, but different support nature and average gold particle diameter. If CO conversion rate was only dependent on the amount of adsorbed oxygen (i.e., density of Au perimeter sites), and assuming that the resulting adsorbed O_2 species on all the supports were the same or had similar activity towards CO oxidation, then it would be expected that the corresponding turnover frequencies (TOFs) normalized per O_2 species (e.g., perimeter sites as found in this work at 398 K) would be similar for all catalysts.

Figure 5 summarizes CO oxidation TOFs normalized per three types of sites, total Au surface sites (TOF-S), total perimeter sites (TOF-P), and only corner sites (TOF-C) at the Au-support perimeter as a function of the particle diameter, *d*. The main findings were:

a) The TOFs that varied the least with Au particle size where those normalized per total surface Au atoms (TOF-S).
b) There was a trend for TOFs *vs d* resulting in two separate correlations depending on the support nature, reducible (solid symbols) and non-reducible (filled symbols).
c) TOFs were higher for gold catalysts with reducible supports than nonreducible supports.

The similarity of TOF-S (finding a) suggests that at the studied conditions CO oxidation is not limited by the availability of O_2 species at the periphery, but by the availability of total Au surface atoms. Thus, it is likely that CO molecules adsorbed on the gold NP surface limit CO oxidation as they need to diffuse to the reaction zone at the perimeter sites where oxygen is present [13, 14]. The different correlation for TOF-S for reducible *vs* non-reducible supports (finding b) and the (~one order of magnitude) higher TOF-S for catalysts with reducible supports (finding c) adds more nuance to the above observation (finding a). They suggest a likely decrease in the number of active sites or active species for nonreducible supports, but without change in the mechanism or the rate controlling step. These results agree with prior studies by Fujitani and Nakamura for CO oxidation at a similar reaction temperature (400 K) for Au/TiO_2 with particle sizes in the 1.5-10 nm range, which reported similar TOF-S *vs d* [79]. It is worth noting that Fujitani and Nakamura [79] and Kotobuki et al. [88] also found a similarity of TOF-P at 300 and 353 K, respectively, which points out at the relevance of perimeter sites, but at lower temperatures. The different catalytic performance for catalysts with reducible and non-reducible supports is also well known in gold catalysis [78]. Recent work by Saavedra et al. for CO oxidation on Au/TiO_2 (reducible support) and Au/Al_2O_3 (nonreducible support) catalysts at low temperature (320 K) indicated that the lower activity for the Au/Al_2O_3 catalyst could be attributed to a reduction in the number of active sites as a result of partial carbonate poisoning at the $Au\text{-}Al_2O_3$ perimeter interface [84]. These results shed light into the possible reasons for support effects in CO oxidation, but other hypothesis for support effects cannot be ruled out including the presence of different gold nanoparticle shapes as a result of a strong interaction with support which could introduce new active sites involved in the rate determining step [14, 82] and differences in Au adsorption properties for O_2 [19] and CO [83]. Given the different apparent dependencies on oxygen adsorption at the Au-support perimeter and CO adsorbed on the Au surface, the results suggest that both oxygen and CO are involved in rate determining steps, but limited by the availability of the latter in the reaction zone (Au-support perimeter

interface), on Au for reducible and nonreducible supports. This is in agreement with mechanistic proposals for CO oxidation on Au/TiO_2 and Au/Al_2O_3 by Saavedra et al. [13, 84] and Green et al. [14]. Overall, these results and the use of in situ UV-Vis as a characterization tool for assessment of Au site location of adsorbed species provided additional insights into CO oxidation catalysis by gold and raised new hypothesis which can be further proved or disproved with additional kinetic and in situ spectroscopic experimentation including the UV-vis plasmon resonance methodology reported in this work.

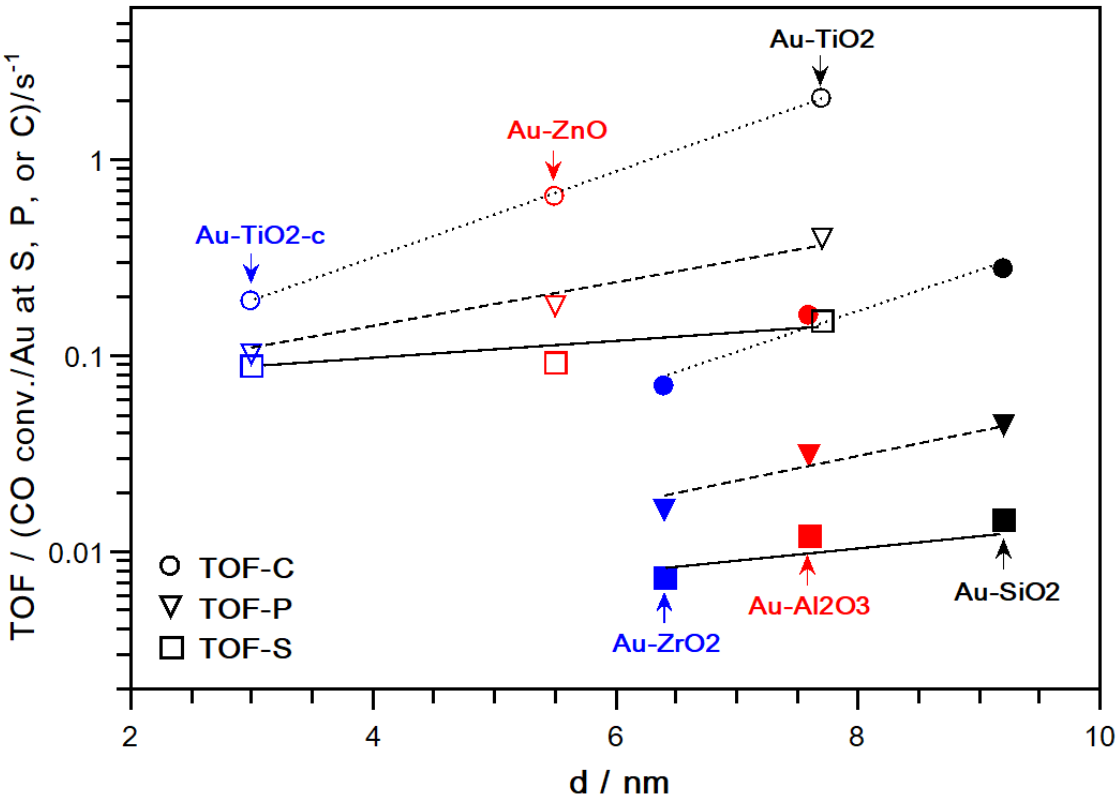

Figure 5. Correlation between Au site normalized turnover frequency (TOF) vs Au average diameter (*d*). TOF defined as the number of molecules of CO converted per second per total number of Au atoms at: 1) the surface (TOF-S; squares, solid lines; dispersion, $D = 0.99/d^{0.83}$); 2) at the Au-support perimeter (TOF-P; triangles, dashed lines, $D = 0.43/d^{1.71}$); and 3) at the perimeter corners (TOF-C; circles, dotted lines, $D = 0.25/d^{2.78}$). Catalysts with reducible supports are identified with empty symbols and nonreducible ones with filled symbols. Each catalyst' results are reported under or above each name (same *d*). Data collected in in situ/operando reaction cell. CO oxidation conditions: 398 K and 101 kPa total pressure (1 kPa

CO, 2 kPa O_2, balance He). CO conversion varied between ~1-25%. Lines added to guide the eye.

In summary, we have prepared Au nanoparticles on various metal oxide supports by means of ammonia deposition-precipitation method. During catalyst preparation in aqueous solution, ammonia interacts strongly with surface hydroxyl groups in the support to form positively charged sites [40]. In the present case, at a pH of 9, the Au precursor ($HAuCl_4$) forms primarily $Au(OH)^{4-}$ anionic gold solution species which adsorb preferentially in the ammonia anchor sites on the support (**Figure 5**, steps 1-2) [41]. A heat treatment at high temperature (HT usually >573 K) in air (i.e., calcination) is typically required to form highly dispersed Au nanoparticles on the support (**Figure 5**, step 3) [6, 41]. After this calcination treatment, some O_2 species from air will remain adsorbed on the catalyst, which can be removed by treatment in H_2 flow at high temperature (commonly ~473-573 K) (**Figure 5**, step 4), preparing the catalyst surface for reaction or further treatments. In the present work, Au nanoparticles supported on various metal oxides (i.e., SiO_2, Al_2O_3, ZrO_2, ZnO, and TiO_2) were pretreated in such fashion and then submitted to sequential O_2-He-H_2-He-O_2 gas treatments (**Figure 5**, step 5-7). During these exposures to O_2 and H_2, some O and H containing species form and remain adsorbed on the catalyst surface, but whose actual nature (e.g., OH, OOH, O_2, O_2^-, O^-, O^{2-}, etc) is currently unknown and thus are noted as O_x and H_y in **Figure 5**. Upon data analysis of the Au plasmon peak position changes, the in situ UV-vis results showed evidence for adsorption of O_2 and H_2 derived species at the Au-support perimeter at a relatively high temperature (398 K) during O_2 and H_2 flowing conditions and after flushing with He.

The present application of in situ gold plasmon sensing of adsorbed O_2 and H_2 to inquire about adsorption site location on supported gold catalysts is quite notable since very small amounts of adsorbed O_2 and H_2 cause measurable and reproducible Au plasmon peak position shifts in gold catalysts with nanoparticle diameters relevant for catalysis (*d* 3-9 nm), which makes the technique amenable to systematic studies of other properties that can affect O_2 and H_2 adsorption such as support morphology, acidity/basicity, and composition including the presence of promoters/dopants and mixed metal oxides, among others. Such applications could be even expanded to very low gas phase concentrations as demonstrated for sensing of H_2 (100-1000 ppm), CO (20-2000 ppm), or NO_2 (2-100 ppm) on thin films of Au/TiO_2 [89], Au/YSZ [24, 89],

and Au/CeO_2 [25, 89]. A methodology relating the dependence of the coordination of Au atoms (from site statistics) as a function of particle size with catalytic activity (but not with spectroscopic data) was reported for CO oxidation [70] and the water-gas shift reaction [67]. The method described here expands the application of site statistics correlations to in situ spectroscopic data at relevant reaction conditions demonstrating its utility to understand adsorbed species on catalyst active sites in their working state giving unprecedented access to adsorption sites location on practical catalysts. Moreover, the in situ gold plasmon technique has the potential for widespread use as it can be applied directly to powder catalysts that exhibit plasmon resonance (e.g., Au, Ag, Cu) requiring a relatively inexpensive reaction setup and in situ reaction cell [33, 90].

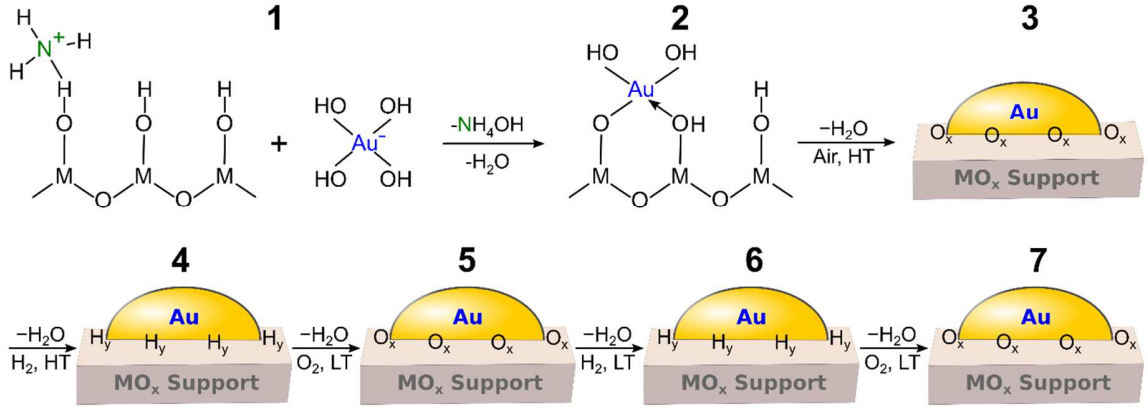

Figure 5. Proposed schematic representation of supported Au nanoparticles prepared by deposition-precipitation method with ammonia and their interaction with O_2 and H_2.

In a specific example, the catalytic activity of the prepared catalysts in CO oxidation at 398 K did not correlate with Au-support perimeter interface (as expected if the conversion rate was only limited by the density of Au-support perimeter sites, i.e., adsorbed O_2 amount), but rather it correlated with the total Au surface atoms where CO can adsorb. This activity was also different for catalysts prepared with reducible and nonreducible supports. Based on these results and prior reports, we hypothesize that support surface properties, including reducibility and acid-base properties, can affect the nature and density of active sites and adsorbed species derived from reactants and products resulting in more or less active oxidation catalysts. These preliminary catalytic results clearly show that more systematic and combined kinetic and in situ spectroscopic studies, including the spectroscopic analysis of adsorption sites location, are

required to shed light into the controlling mechanisms for oxidation reactions on reducible and nonreducible supports, over a wide range of Au NP sizes, and a variety of reaction conditions (e.g., low *vs* high temperature, in presence/absence of co-fed water, etc).

4. Conclusions

An in situ UV-vis gold plasmon sensing methodology was developed to investigate O_2 and H_2 adsorption properties of supported gold catalysts. The technique was applied at conditions relevant to catalysis (e.g., 398 K and flowing O_2 and H_2) and in combination with Au nanoparticle site statistics analysis provided the first in situ UV-Vis spectroscopic evidence for adsorption of O_2 and H_2 at undercoordinated Au sites predominantly located at Au-support perimeter sites. The technique is based on monitoring the changes of the Au surface plasmon peak position in real time in an in situ/operando diffuse reflectance UV-Vis reaction cell under oxidizing (e.g., O_2), reducing (e.g., H_2), and inert (e.g., He) environments. The Au catalysts were prepared by the deposition-precipitation method using ammonia as the base reagent to minimize sodium contamination in the catalysts, to prepare catalysts with similar Au content, and supported on metal oxides of close surface area including SiO_2, Al_2O_3, ZrO_2, ZnO, and TiO_2. This synthetic methodology allowed us to reduce the number of experimental variables to probe the catalysts for O_2 and H_2 adsorption at relatively high temperature (398 K). A key to the development of the methodology was the use of a Drude-Lorentz model for gold nanoparticles employed to estimate the relative charge transfer change from/to gold during O_2 or H_2 adsorption and titration with H_2 or O_2, respectively. This relative charge transfer change, estimated from in situ UV-Vis spectroscopic data (i.e., Au plasmon peak position), was used as a proxy of adsorbed O_2 or H_2 species to correlate with gold adsorption sites. It was found that, regardless of the support nature, O_2 or H_2 adsorption at 398 K primarily occurred at Au-support perimeter sites thus stressing the important role of particle size in gold catalysis as a possible catalyst design parameter.

The prepared catalysts were evaluated for CO oxidation at 398 K. It was found that CO oxidation turnover frequencies showed distinct linear trends for reducible and nonreducible supports, which were less dependent on gold particle size when normalized by the total number of gold surface atoms. Overall, the plasmon and catalytic activity results provided evidence of oxygen species adsorption at the Au-support perimeter and CO or CO_x intermediate species

adsorbed on all surface gold atoms, the latter which seem to control conversion rates on reducible and nonreducible supports. These findings raise additional questions regarding CO oxidation mechanism and enhancement of catalytic activity at a variety of conditions since adsorbed oxygen species do not seem to limit catalytic activity at relatively high temperatures. Future work with the Au plasmon technique in combination with kinetic and in situ/operando spectroscopies (e.g., IR, Raman) should shed additional light to our understanding of metal-support effects, particle size, and reactant/product inhibition in CO and other oxidation and hydrogenation reactions enabled by gold catalysts.

Acknowledgments

The authors acknowledge financial support by the National Science Foundation under grants No OIA-1539105 and CBET-1847655, and by the University of Kansas through the New Faculty General Research Fund award #2302093. W.R. Grace is also acknowledged for donation of the SiO_2 (Davisil XWP 1000A) sample.

Appendix A. Supplementary data

Supplementary data associated with this article can be found in the online version, at https://dx.doi.org/

Acronyms

AP-XPS	Ambient pressure X-ray photoelectron spectroscopy
CCD	Charge coupled device
CN	Coordination number
CT	Charge transfer
DFT	Density functional theory
DP	Deposition-precipitation
EPR	Electron paramagnetic resonance
ETEM	Environmental transmission electron microscopy
EXAFS	Extended X-ray absorption fine structure
HT	High temperature
FTIR	Fourier transform infrared
NP	Nanoparticle
SPR	Surface plasmon resonance
SEM-EDX	Scanning electron microscopy - energy dispersive X-ray
TAP	Temporal analysis of products
TEM	Transmission electron microscopy
TOF	Turnover frequency

TOF-C	Turnover frequency normalized per perimeter corner Au surface atoms
TOF-P	Turnover frequency normalized per total perimeter Au surface atoms
TOF-S	Turnover frequency normalized per total Au surface atoms
TPR/TPO	Temperature programmed reduction/oxidation
UHP	Ultra-high purity
UV-Vis	Ultraviolet-Visible
XANES	X-ray absorption near edge structure
XRD	X-ray diffraction
YSZ	Yttria-stabilized zirconia

Table of Symbols

a, b, c	Nanospheroid semi-axes
c	Speed of light, in vacuum: 299792458 m/s
$\boldsymbol{C_{abs}}$	Absorption cross-section
d	Average metal nanoparticle size (nm)
D	Dispersion
$\boldsymbol{F(R_\infty)}$	Kubelka-Munk function
K	Absorption coefficient
L	Nanoparticle geometrical factor (e.g., for a sphere a=b=c and L=1/3)
$\boldsymbol{m}$	Mass of the electron, $9.10938291 \times 10^{-31}$ kg
N	Conduction electron density
$\boldsymbol{N_{Au}}$	Number of Au nanoparticles per unit volume
$\boldsymbol{\Delta N}$	Change in the conduction electron density
$\boldsymbol{\Delta N/N}$	Relative change in charge transfer
r	Average particle radius
S	Scattering coefficient
$\boldsymbol{\alpha}$	Polarizability
e	Electron charge, $1.60217657 \times 10^{-19}$ C
$\boldsymbol{\varepsilon_0}$	Permittivity of vacuum, $8.854187817 \times 10^{-12}$ C/Vm
$\boldsymbol{\epsilon}$	Dielectric function
$\boldsymbol{\epsilon_1}$	Real part of the dielectric function
$\boldsymbol{\epsilon_2}$	Imaginary part of the dielectric function
$\boldsymbol{\epsilon_\infty}$	Offset constant
$\boldsymbol{\epsilon_b}$	Bound (interband) electron contribution to the dielectric function
$\boldsymbol{\epsilon_f}$	Free (intraband) electron contribution to the dielectric function
$\boldsymbol{\epsilon_m}$	Dielectric function of the surrounding medium
$\boldsymbol{\gamma_b}$	Damping constant for bound electrons
$\boldsymbol{\gamma_f}$	Damping constant for free electrons
λ	Photon wavelength (or shifted plasmon wavelength after charge transfer)
$\boldsymbol{\lambda_m}$	Photon wavelength at which plasmon maximum absorption occurs (corresponding to the initial reference charge density N)
Δλ	Relative change in plasmon peak position
$\boldsymbol{\omega}$	Impinging wave frequency ($\boldsymbol{\omega = 2\pi c/\lambda}$)
$\boldsymbol{\omega_0}$	Oscillation frequency of a bound electron under an electric field

$\boldsymbol{\omega_p}$	Plasma frequency of the bulk metal given by $\boldsymbol{\omega_p^2 = Ne^2/m\varepsilon_0}$
$\boldsymbol{R_\infty}$	Reflectance

References

[1] G.C. Bond, P.A. Sermon, G. Webb, D.A. Buchanan, P.B. Wells, Hydrogenation over supported gold catalysts, J. Chem. Soc., Chem. Commun., (1973), 444-445

[2] B. Nkosi, N.J. Coville, G.J. Hutchings, Reactivation of a supported gold catalyst for acetylene hydrochlorination, J. Chem. Soc., Chem. Commun., (1988), 71-72

[3] M. Haruta, T. Kobayashi, H. Sano, N. Yamada, Novel gold catalysts for the oxidation of carbon monoxide at a temperature far below 0 °c, Chem. Lett., 16 (1987), 405-408

[4] T. Hayashi, K. Tanaka, M. Haruta, Selective vapor-phase epoxidation of propylene over Au/TiO2 catalysts in the presence of oxygen and hydrogen, J. Catal., 178 (1998), 566-575

[5] L. Prati, M. Rossi, Gold on carbon as a new catalyst for selective liquid phase oxidation of diols, J. Catal., 176 (1998), 552-560

[6] T. Takei, T. Akita, I. Nakamura, T. Fujitani, M. Okumura, K. Okazaki, J.H. Huang, T. Ishida, M. Haruta, Heterogeneous catalysis by gold, Adv. Catal., 55 (2012), 1-126

[7] S.W. Zeng, D. Baillargeat, H.P. Ho, K.T. Yong, Nanomaterials enhanced surface plasmon resonance for biological and chemical sensing applications, Chem. Soc. Rev., 43 (2014), 3426-3452

[8] S. Linic, U. Aslam, C. Boerigter, M. Morabito, Photochemical transformations on plasmonic metal nanoparticles, Nat. Mater., 14 (2015), 567-576

[9] U. Kreibig, M. Vollmer, Optical properties of metal clusters, Springer: Berlin (Germany), 1995; pp 1-553

[10] J.J. Bravo-Suárez, R.V. Chaudhari, B. Subramaniam, Design of heterogeneous catalysts for fuels and chemicals processing: An overview. In: Novel materials for catalysis and fuels processing; Bravo-Suárez, J.J.;Kidder, M.K.;Schwartz, V. Eds.; American Chemical Society: Washington, D.C., 2013; pp. 3-68

[11] J.J. Bravo-Suárez, K.K. Bando, J.I. Lu, M. Haruta, T. Fujitani, S.T. Oyama, Transient technique for identification of true reaction intermediates: Hydroperoxide species in propylene epoxidation on gold/titanosilicate catalysts by X-ray absorption fine structure spectroscopy, J. Phys. Chem. C, 112 (2008), 1115-1123

[12] S.T. Oyama, W. Zhang, True and spectator intermediates in catalysis: The case of ethanol oxidation on molybdenum oxide as observed by in situ laser Raman spectroscopy, J. Am. Chem. Soc., 118 (1996), 7173-7177

[13] J. Saavedra, H.A. Doan, C.J. Pursell, L.C. Grabow, B.D. Chandler, The critical role of water at the gold-titania interface in catalytic CO oxidation, Science, 345 (2014), 1599-1602

[14] I.X. Green, W.J. Tang, M. Neurock, J.T. Yates, Spectroscopic observation of dual catalytic sites during oxidation of CO on a Au/TiO2 catalyst, Science, 333 (2011), 736-739

[15] C. Schilling, C. Hess, CO oxidation on ceria supported gold catalysts studied by combined operando Raman/UV-Vis and IR spectroscopy, Top. Catal., 60 (2017), 131-140

[16] J.A. van Bokhoven, C. Louis, J. T Miller, M. Tromp, O.V. Safonova, P. Glatzel, Activation of oxygen on gold/alumina catalysts: In situ high-energy-resolution fluorescence and time-resolved X-ray spectroscopy, Angew. Chem., Int. Ed., 45 (2006), 4651-4654

[17] N. Weiher, A.M. Beesley, N. Tsapatsaris, L. Delannoy, C. Louis, J.A. van Bokhoven, S.L.M. Schroeder, Activation of oxygen by metallic gold in Au/TiO2 catalysts, J. Am. Chem. Soc., 129 (2007), 2240-2241

[18] D. Widmann, Y. Liu, F. Schuth, R.J. Behm, Support effects in the Au-catalyzed CO oxidation - correlation between activity, oxygen storage capacity, and support reducibility, J. Catal., 276 (2010), 292-305

[19] D. Widmann, R.J. Behm, Activation of molecular oxygen and the nature of the active oxygen species for CO oxidation on oxide supported Au catalysts, Acc. Chem. Res., 47 (2014), 740-749

[20] P. Lakshmanan, F. Averseng, N. Bion, L. Delannoy, J.M. Tatibouet, C. Louis, Understanding of the oxygen activation on ceria- and ceria/alumina-supported gold

catalysts: A study combining O-18/O-16 isotopic exchange and EPR spectroscopy, Gold Bull., 46 (2013), 233-242

[21] J.J. Bravo-Suárez, K.K. Bando, T. Akita, T. Fujitani, T.J. Fuhrer, S.T. Oyama, Propane reacts with O-2 and H-2 on gold supported TS-1 to form oxygenates with high selectivity, Chem. Commun. (Cambridge, U. K.), (2008), 3272-3274

[22] J.J. Bravo-Suárez, K.K. Bando, T. Fujitani, S.T. Oyama, Mechanistic study of propane selective oxidation with H-2 and O-2 on Au/TS-1, J. Catal., 257 (2008), 32-42

[23] J.J. Bravo-Suárez, K.K. Bando, J. Lu, T. Fujitani, S.T. Oyama, Oxidation of propane to propylene oxide on gold catalysts, J. Catal., 255 (2008), 114-126

[24] P.H. Rogers, G. Sirinakis, M.A. Carpenter, Direct observations of electrochemical reactions within Au-YSZ thin films via absorption shifts in the an nanoparticle surface plasmon resonance, J. Phys. Chem. C, 112 (2008), 6749-6757

[25] N.A. Joy, M.I. Nandasiri, P.H. Rogers, W.L. Jiang, T. Varga, S. Kuchibhatla, S. Thevuthasan, M.A. Carpenter, Selective plasmonic gas sensing: H-2, NO2, and CO spectral discrimination by a single Au-CeO2 nanocomposite film, Anal. Chem., 84 (2012), 5025-5034

[26] P.R. Ohodnicki, M.P. Buric, T.D. Brown, C. Matranga, C.J. Wang, J. Baltrus, M. Andio, Plasmonic nanocomposite thin film enabled fiber optic sensors for simultaneous gas and temperature sensing at extreme temperatures, Nanoscale, 5 (2013), 9030-9039

[27] P.R. Ohodnicki, T.D. Brown, G.R. Holcomb, J. Tylczak, A.M. Schultz, J.P. Baltrus, High temperature optical sensing of gas and temperature using Au-nanoparticle incorporated oxides, Sens. Actuators, B, 202 (2014), 489-499

[28] Y. Borensztein, L. Delannoy, A. Djedidi, R.G. Barrera, C. Louis, Monitoring of the plasmon resonance of gold nanoparticles in Au/TiO2 catalyst under oxidative and reducing atmospheres, J. Phys. Chem. C, 114 (2010), 9008-9021

[29] Y. Borensztein, L. Delannoy, R.G. Barrera, C. Louis, Kinetics of the plasmon optical response of Au nanoparticles/TiO2 catalyst under O-2 and H-2 followed by differential diffuse reflectance spectroscopy, Eur. Phys. J. D, 63 (2011), 235-240

[30] E.M. Larsson, C. Langhammer, I. Zorić, B. Kasemo, Nanoplasmonic probes of catalytic reactions, Science, 326 (2009), 1091-1094

[31] C. Langhammer, E.M. Larsson, Nanoplasmonic in situ spectroscopy for catalysis applications, ACS Catal., 2 (2012), 2036-2045

[32] C. Langhammer, E.M. Larsson, B. Kasemo, I. Zoric, Indirect nanoplasmonic sensing: Ultrasensitive experimental platform for nanomaterials science and optical nanocalorimetry, Nano Lett., 10 (2010), 3529-3538

[33] P.D. Srinivasan, S.R. Nitz, K.J. Stephens, E. Atchison, J.J. Bravo-Suárez, Modified harrick reaction cell for in situ/operando fiber optics diffuse reflectance UV–visible spectroscopic characterization of catalysts, Appl. Catal., A, 561 (2018), 7-18

[34] N.A. Joy, C.M. Settens, R.J. Matyi, M.A. Carpenter, Plasmonic based kinetic analysis of hydrogen reactions within Au−YSZ nanocomposites, J. Phys. Chem. C, 115 (2011), 6283-6289

[35] G. Steinhauser, J. Evers, S. Jakob, T.M. Klapötke, G. Oehlinger, A review on fulminating gold (knallgold), Gold Bull., 41 (2008), 305-317

[36] B. Chowdhury, J.J. Bravo-Suárez, N. Mimura, J.Q. Lu, K.K. Bando, S. Tsubota, M. Haruta, In situ UV-vis and EPR study on the formation of hydroperoxide species during direct gas phase propylene epoxidation over Au/Ti-SiO2 catalyst, J. Phys. Chem. B, 110 (2006), 22995-22999

[37] J.J. Bravo-Suárez, J. Lu, C.G. Dallos, T. Fujitani, S.T. Oyama, Kinetic study of propylene epoxidation with H-2 and O-2 over a gold/mesoporous titanosilicate catalyst, J. Phys. Chem. C, 111 (2007), 17427-17436

[38] J.Q. Lu, J.J. Bravo-Suárez, A. Takahashi, M. Haruta, S.T. Oyama, In situ UV-vis studies of the effect of particle size on the epoxidation of ethylene and propylene on supported silver catalysts with molecular oxygen, J. Catal., 232 (2005), 85-95

[39] T.A. Nijhuis, T. Visser, B.M. Weckhuysen, Mechanistic study into the direct epoxidation of propene over gold/titania catalysts, J. Phys. Chem. B, 109 (2005), 19309-19319

[40] N. Phonthammachai, T.J. White, One-step synthesis of highly dispersed gold nanocrystals on silica spheres, Langmuir, 23 (2007), 11421-11424

[41] F. Moreau, G.C. Bond, A.O. Taylor, Gold on titania catalysts for the oxidation of carbon monoxide: Control of ph during preparation with various gold contents, J. Catal., 231 (2005), 105-114

[42] B. Shao, J. Zhang, J. Huang, B. Qiao, Y. Su, S. Miao, Y. Zhou, D. Li, W. Huang, W. Shen, Size-dependency of gold nanoparticles on TiO2 for CO oxidation, Small Methods, 2 (2018), 1800273

[43] X.J. Wei, B. Shao, Y. Zhou, Y. Li, C.C. Jin, J.Y. Liu, W.J. Shen, Geometrical structure of the gold-iron(III) oxide interfacial perimeter for CO oxidation, Angew. Chem., Int. Ed., 57 (2018), 11289-11293

[44] L. Delannoy, R.L. Chantry, S. Casale, Z.Y. Li, Y. Borensztein, C. Louis, HRTEM and STEM-HAADF characterisation of Au-TiO2 and Au-Al2O3 catalysts for a better understanding of the parameters influencing their properties in CO oxidation, Phys. Chem. Chem. Phys., 15 (2013), 3473-3479

[45] Y. Kuwauchi, H. Yoshida, T. Akita, M. Haruta, S. Takeda, Intrinsic catalytic structure of gold nanoparticles supported on TiO2, Angew. Chem., Int. Ed., 51 (2012), 7729-7733

[46] T. Uchiyama, H. Yoshida, Y. Kuwauchi, S. Ichikawa, S. Shimada, M. Haruta, S. Takeda, Systematic morphology changes of gold nanoparticles supported on CeO2 during CO oxidation, Angew. Chem., Int. Ed., 50 (2011), 10157-10160

[47] A.S. Barnard, X.M. Lin, L.A. Curtiss, Equilibrium morphology of face-centered cubic gold nanoparticles >3 nm and the shape changes induced by temperature, J. Phys. Chem. B, 109 (2005), 24465-24472

[48] A.S. Barnard, L.A. Curtiss, Predicting the shape and structure of face-centered cubic gold nanocrystals smaller than 3 nm, ChemPhysChem, 7 (2006), 1544-1553

[49] F.C. Jentoft, Ultraviolet–Visible–near infrared spectroscopy in catalysis: Theory, experiment, analysis, and application under reaction conditions, Adv. Catal., 52 (2009), 129-211

[50] J.J. Bravo-Suárez, P.D. Srinivasan, Design characteristics of in situ and operando ultraviolet-visible and vibrational spectroscopic reaction cells for heterogeneous catalysis, Catal. Rev.- Sci. Eng., 59 (2017), 295-445

[51] C.F. Bohren, D.R. Huffman, Absorption and scattering of light by small particles, Wiley, 1983; pp 1-533

[52] Y. Li, Chapter 1: Optical properties of plasmonic materials. In: Plasmonic optics: Theory and applications; Eds.; SPIE Press, 2017; pp. 1-39

[53] W.L. Watkins, Y. Borensztein, Mechanism of hydrogen adsorption on gold nanoparticles and charge transfer probed by anisotropic surface plasmon resonance, Phys. Chem. Chem. Phys., 19 (2017), 27397-27405

[54] P. Mulvaney, J. Pérez-Juste, M. Giersig, L.M. Liz-Marzán, C. Pecharromán, Drastic surface plasmon mode shifts in gold nanorods due to electron charging, Plasmonics, 1 (2006), 61-66

[55] P. Mulvaney, Surface plasmon spectroscopy of nanosized metal particles, Langmuir, 12 (1996), 788-800

[56] S.S.E. Collins, M. Cittadini, C. Pecharroman, A. Martucci, P. Mulvaney, Hydrogen spillover between single gold nanorods and metal oxide supports: A surface plasmon spectroscopy study, ACS Nano, 9 (2015), 7846-7856

[57] F. Romero-Sarria, J.J. Plata, O.H. Laguna, A.M. Marquez, M.A. Centeno, J.F. Sanz, J.A. Odriozola, Surface oxygen vacancies in gold based catalysts for CO oxidation, RSC Adv., 4 (2014), 13145-13152

[58] S. Takagi, J.-i. Hoshino, H. Tomono, K. Tsumuraya, Electron transfer from hydrogen molecule to Au(111) during dissociative adsorption: A first-principles study, J. Phys. Soc. Jpn., 77 (2008), 054705

[59] K.-S. Lee, M.A. El-Sayed, Gold and silver nanoparticles in sensing and imaging: Sensitivity of plasmon response to size, shape, and metal composition, J. Phys. Chem. B, 110 (2006), 19220-19225

[60] L. Barrio, P. Liu, J.A. Rodriguez, J.M. Campos-Martin, J.L.G. Fierro, Effects of hydrogen on the reactivity of O-2 toward gold nanoparticles and surfaces, J. Phys. Chem. C, 111 (2007), 19001-19008

[61] K.J. Sun, M. Kohyama, S. Tanaka, S. Takeda, A study on the mechanism for H-2 dissociation on Au/TiO2 catalysts, J. Phys. Chem. C, 118 (2014), 1611-1617

[62] J.M. Herrmann, The electronic factor and related redox processes in oxidation catalysis, Catal. Today, 112 (2006), 73-77

[63] J.C. Fierro-Gonzalez, B.C. Gates, Catalysis by gold dispersed on supports: The importance of cationic gold, Chem. Soc. Rev., 37 (2008), 2127-2134

[64] J.E. Benson, M. Boudart, Hydrogen-oxygen titration method for the measurement of supported platinum surface areas, J. Catal., 4 (1965), 704-710

[65] H. Berndt, I. Pitsch, S. Evert, K. Struve, M.M. Pohl, J. Radnik, A. Martin, Oxygen adsorption on Au/Al2O3 catalysts and relation to the catalytic oxidation of ethylene glycol to glycolic acid, Appl. Catal., A, 244 (2003), 169-179

[66] M. Haruta, Size- and support-dependency in the catalysis of gold, Catal. Today, 36 (1997), 153-166

[67] M. Shekhar, J. Wang, W.S. Lee, W.D. Williams, S.M. Kim, E.A. Stach, J.T. Miller, W.N. Delgass, F.H. Ribeiro, Size and support effects for the water-gas shift catalysis over gold nanoparticles supported on model Al2O3 and TiO2, J. Am. Chem. Soc., 134 (2012), 4700-4708

[68] A. Carlsson, A. Puig-Molina, T.V.W. Janssens, New method for analysis of nanoparticle geometry in supported fcc metal catalysts with scanning transmission electron microscopy, J. Phys. Chem. B, 110 (2006), 5286-5293

[69] A. Ruiz Puigdollers, P. Schlexer, S. Tosoni, G. Pacchioni, Increasing oxide reducibility: The role of metal/oxide interfaces in the formation of oxygen vacancies, ACS Catal., 7 (2017), 6493-6513

[70] T.V.W. Janssens, B.S. Clausen, B. Hvolbaek, H. Falsig, C.H. Christensen, T. Bligaard, J.K. Norskov, Insights into the reactivity of supported Au nanoparticles: Combining theory and experiments, Top. Catal., 44 (2007), 15-26

[71] Y.Y. Wu, N.A. Mashayekhi, H.H. Kung, Au-metal oxide support interface as catalytic active sites, Catal. Sci. Technol., 3 (2013), 2881-2891

[72] I.X. Green, W.J. Tang, M. Neurock, J.T. Yates, Low-temperature catalytic H-2 oxidation over Au nanoparticle/TiO2 dual perimeter sites, Angew. Chem., Int. Ed., 50 (2011), 10186-10189

[73] T. Whittaker, K.B.S. Kumar, C. Peterson, M.N. Pollock, L.C. Grabow, B.D. Chandler, H-2 oxidation over supported Au nanoparticle catalysts: Evidence for heterolytic H-2 activation at the metal-support interface, J. Am. Chem. Soc., 140 (2018), 16469-16487

[74] T. Fujitani, I. Nakamura, T. Akita, M. Okumura, M. Haruta, Hydrogen dissociation by gold clusters, Angew. Chem., Int. Ed., 48 (2009), 9515-9518

[75] A. Brückner, Electron paramagnetic resonance: A powerful tool for monitoring working catalysts. In: Adv. Catal.; Gates, B.C.;Knözinger, H. Eds.; Academic Press, 2007; pp. 265-308

[76] C. Lamberti, A. Zecchina, E. Groppo, S. Bordiga, Probing the surfaces of heterogeneous catalysts by in situ IR spectroscopy, Chem. Soc. Rev., 39 (2010), 4951-5001

[77] P. Jiang, S. Porsgaard, F. Borondics, M. Köber, A. Caballero, H. Bluhm, F. Besenbacher, M. Salmeron, Room-temperature reaction of oxygen with gold: An in situ ambient-pressure X-ray photoelectron spectroscopy investigation, J. Am. Chem. Soc., 132 (2010), 2858-2859

[78] M. Haruta, Spiers memorial lecture role of perimeter interfaces in catalysis by gold nanoparticles, Faraday Discuss., 152 (2011), 11-32

[79] T. Fujitani, I. Nakamura, Mechanism and active sites of the oxidation of CO over Au/TiO2, Angew. Chem., Int. Ed., 50 (2011), 10144-10147

[80] V. Aguilar-Guerrero, B.C. Gates, Kinetics of CO oxidation catalyzed by supported gold: A tabular summary of the literature, Catal. Lett., 130 (2009), 108-120

[81] S.H. Overbury, V. Schwartz, D.R. Mullins, W. Yan, S. Dai, Evaluation of the Au size effect: CO oxidation catalyzed by Au/TiO2, J. Catal., 241 (2006), 56-65

[82] M. Comotti, W.C. Li, B. Spliethoff, F. Schuth, Support effect in high activity gold catalysts for CO oxidation, J. Am. Chem. Soc., 128 (2006), 917-924

[83] Y. Wang, D. Widmann, M. Heenemann, T. Diemant, J. Biskupek, R. Schlogl, R.J. Behm, The role of electronic metal-support interactions and its temperature dependence: CO adsorption and CO oxidation on Au/TiO2 catalysts in the presence of TiO2 bulk defects, J. Catal., 354 (2017), 46-60

[84] J. Saavedra, C.J. Pursell, B.D. Chandler, CO oxidation kinetics over Au/TiO2 and Au/Al2O3 catalysts: Evidence for a common water-assisted mechanism, J. Am. Chem. Soc., 140 (2018), 3712-3723

[85] J.C. Clark, S. Dai, S.H. Overbury, Operando studies of desorption, reaction and carbonate formation during CO oxidation by Au/TiO2 catalysts, Catal. Today, 126 (2007), 135-142

[86] B.K. Chang, B.W. Jang, S. Dai, S.H. Overbury, Transient studies of the mechanisms of CO oxidation over Au/TiO2 using time-resolved FTIR spectroscopy and product analysis, J. Catal., 236 (2005), 392-400

[87] J.M.C. Soares, M. Hall, M. Cristofolini, M. Bowker, The role of impurities on the low temperature CO oxidation on Au/TiO2, Catal. Lett., 109 (2006), 103-108

[88] M. Kotobuki, R. Leppelt, D.A. Hansgen, D. Widmann, R.J. Behm, Reactive oxygen on a Au/TiO2 supported catalyst, J. Catal., 264 (2009), 67-76

[89] N.A. Joy, P.H. Rogers, M.I. Nandasiri, S. Thevuthasan, M.A. Carpenter, Plasmonic-based sensing using an array of Au–metal oxide thin films, Anal. Chem., 84 (2012), 10437-10444

[90] B.S. Patil, P.D. Srinivasan, E. Atchison, H. Zhu, J.J. Bravo-Suárez, Design, modelling, and application of a low void-volume in situ diffuse reflectance spectroscopic reaction cell for transient catalytic studies, React. Eng. Chem., 4 (2019), 667-678

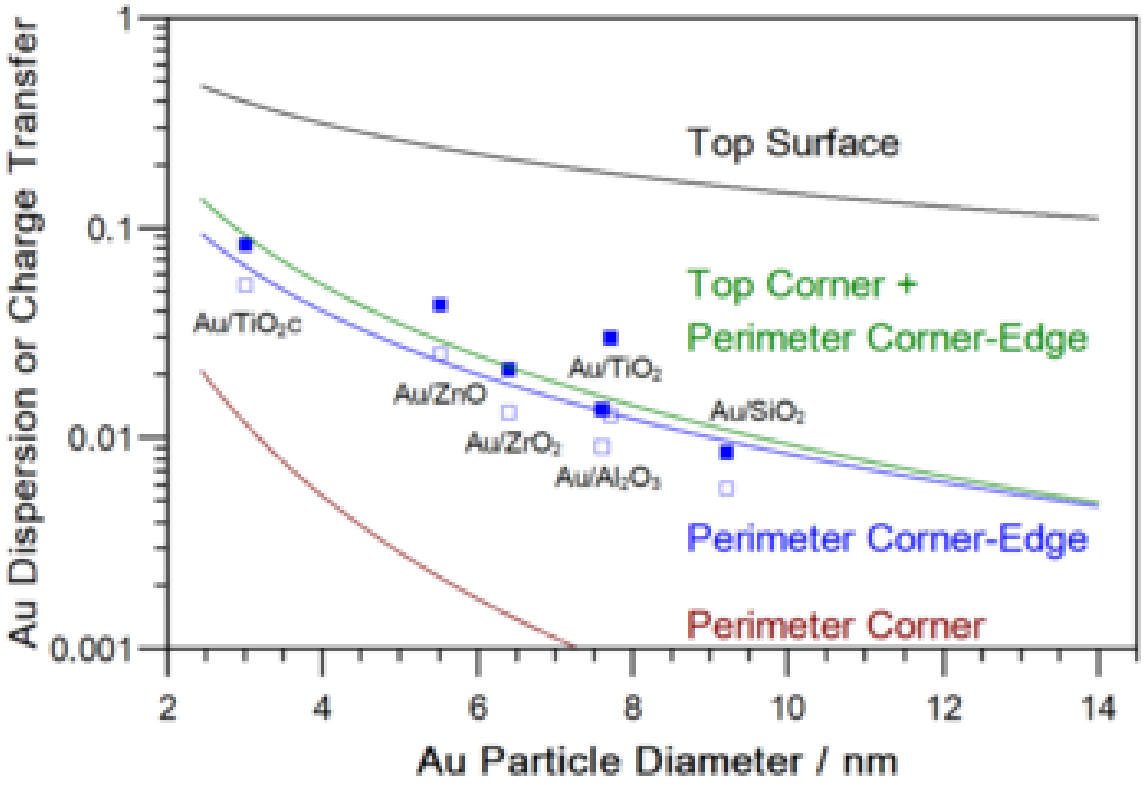
Au Dispersion or Charge Transfer
1
0.1
0.01
0.001
2
4
6
8
10
12
14
Au Particle Diameter / nm
Top Surface
Top Corner +
Perimeter Corner-Edge
Perimeter Corner-Edge
Perimeter Corner
Au/TiO2c
Au/TiO2
Au/ZnO
Au/SiO2
Au/ZrO2
Au/Al2O3

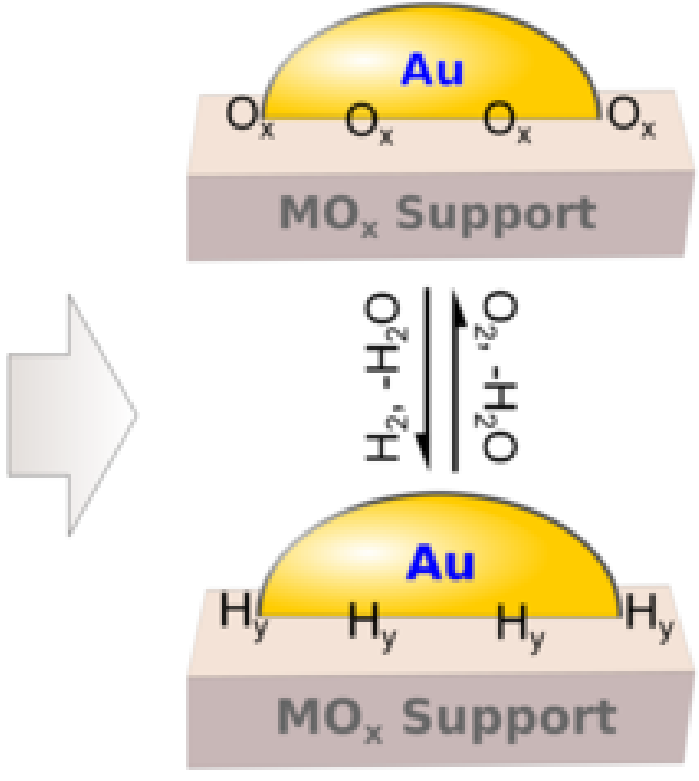
Au
Ox
Ox
Ox
Ox
MOx Support
H2, -H2O
O2, -H2O
Au
Hy
Hy
Hy
Hy
MOx Support